Activated iPSC-microglia from C9orf72 ALS/FTD patients exhibit endosomal-lysosomal dysfunction

Ileana Lorenzini[1], Eric Alsop[2], Jennifer Levy[1], Lauren M Gittings[1], Benjamin E Rabichow[1], Deepti Lall[3], Stephen Moore[1,4], Lynette Bustos[1,4], Ryan Pevey[1,4], Camelia Burciu[1], Justin Saul[1], Amanda McQuade[5,6,7], Makis Tzioras[8,9], Thomas A Mota[3], Amber Logemann[2], Jamie Rose[8,9], Sandra Almeida[10], Fen-Biao Gao[10], Robert Bowser[1], Tara Spires-Jones[8,9], Mathew Blurton-Jones[5,6,7], Tania F Gendron[11,12], Robert H Baloh[3,13], Kendall Van Keuren-Jensen[2], Rita Sattler[1*].

[1]Department of Neurobiology, Barrow Neurological Institute, 350 West Thomas Road Phoenix, AZ 85013, USA.

[2]Neurogenomics Division, Translational Genomics Research Institute, Phoenix, AZ 85004, USA.

[3]Center for Neural Science and Medicine, Regenerative Medicine Institute, Cedars-Sinai Medical Center, Los Angeles, CA 90048, USA.

[4]School of Life Sciences, Arizona State University, Tempe, AZ 85281, USA

[5]Department of Neurobiology and Behavior, University of California Irvine, Irvine, CA 92697, USA

[6]Sue and Bill Gross Stem Cell Research Center, University of California Irvine, Irvine, CA 92697, USA

[7]Institute for Memory Impairments and Neurological Disorders, University of California Irvine, Irvine, CA 92697, USA

[8]UK Dementia Research Institute, The University of Edinburgh, UK

[9]Centre for Brain Discovery Sciences, The University of Edinburgh, UK

[10]Department of Neurology, University of Massachusetts Medical School, Worcester, MA 01655 USA

[11]Department of Neuroscience, Mayo Clinic Jacksonville, FL 32224, USA.

[12]Mayo Clinic Graduate School of Biomedical Sciences, Mayo Clinic, Jacksonville, FL 32224, USA

[13]Department of Neurology, Cedars-Sinai Medical Center, Los Angeles, CA 90048, USA.

*Corresponding author email: rita.sattler@dignityhealth.org

Abstract

Background: A mutation in the *C9orf72* gene is the most common genetic mutation of familial and sporadic ALS, as well as familial FTD. While prior studies have focused on elucidating the mechanisms of neuronal dysfunction and neurodegeneration associated with this genetic mutation, the contribution of microglia to disease pathogenesis in the ALS/FTD disease spectrum remains poorly understood.

Methods: Here, we generated a new disease model consisting of cultured *C9orf72* ALS/FTD patient-derived induced pluripotent stem cells differentiated into microglia (iPSC-MG). We used this model to study the intrinsic cellular and molecular phenotypes of microglia triggered by the *C9orf72* gene mutation.

Results: We show that *C9orf72* ALS/FTD iPSC-MG have a similar transcriptional profile compared to control iPSC-MG, despite the presence of *C9orf72*-associated phenotypes including reduced C9orf72 protein levels and dipeptide-repeat protein translation. Interestingly, *C9orf72* ALS/FTD iPSC-MG exhibit intrinsic dysfunction of phagocytic activity upon exposure to Aβ or brain synaptoneurosomes and display a heightened inflammatory response. Detailed analysis of the endosomal and lysosomal pathways revealed altered expression of endosomal marker early endosome antigen 1 and lysosomal associated membrane protein 1 in *C9orf72* ALS/FTD iPSC-MG, which was confirmed in patient postmortem tissues.

Conclusions: These findings demonstrate that unstimulated *C9orf72* iPSC-MG mono-cultures share a largely similar transcriptome profile with control microglia, despite the presence of *C9orf72* disease phenotypes. The dysfunction of the endosomal-lysosomal pathway as demonstrated by aberrant microglia phagocytosis and engulfment of cellular debris and brain

pathogens suggests that disease-related microglia phenotypes are not intrinsic but instead require microglia to be activated. In summary, the *C9orf72* iPSC-MG culture system provides a novel human disease model to study the role of microglia in *C9orf72* ALS/FTD disease pathogenesis.

Keywords

C9orf72, Amyotrophic Lateral Sclerosis, Frontotemporal Dementia, iPSC, iPSC-microglia, neuroinflammation, microglia, lysosome, endosome

Background

The GGGGCC hexanucleotide repeat expansion (HRE) in the non-coding region of the *chromosome 9 open reading frame 72* (*C9orf72)* gene is considered the most prevalent genetic abnormality associated with amyotrophic lateral sclerosis/frontotemporal dementia (ALS/FTD) to date (1, 2). The *C9orf72* HRE has been hypothesized to contribute to neurodegeneration through three non-mutually exclusive mechanisms. First, *C9orf72* HRE leads to haploinsufficiency and reduced C9orf72 protein expression due to a failure in transcription of the expanded allele; second, non-canonical translation of the repeat RNA leads to synthesis of dipeptide repeat (DPR) proteins; third, RNA toxicity via sequestration of RNA binding proteins to GGGGCC RNA foci. Additionally, *C9orf72* postmortem tissues exhibit TAR-DNA binding protein 43 (TDP-43) pathology, which is characterized by nuclear depletion of TDP-43 and cytoplasmic inclusions, and which is described not only in ALS and FTD, but also in other neurodegenerative diseases, including Alzheimer's disease (AD) and related dementias (3-8).

While neuronal degeneration is a hallmark of ALS and FTD, it is well known that central nervous system (CNS) glia can impact the onset and progression of diseases via non-cell autonomous disease mechanisms (9-16). Microglia are the innate immune cells of the CNS responsible for removing brain pathogens and injury-related debris and are essential to brain development, homeostasis, ageing and disease (17-23). Despite recent investigations, the role of microglia in *C9orf72* ALS/FTD remains poorly understood (24-27). Initial studies using *C9orf72* ALS/FTD postmortem brain tissues revealed more extensive microglia pathology in the corticospinal tract compared to non-*C9orf72* ALS patients (28). The same group also found that microglia activation was significantly higher in ALS patients with dementia or impaired executive function, suggesting that microglia activation correlates with FTD-like symptoms (29). Additional studies reported enlarged lysosomes in microglia in the motor cortex and spinal cord of *C9orf72* ALS patients compared to sporadic ALS (sALS) patients (30). Examination of microglia in postmortem brain tissues from patients with frontotemporal lobar degeneration revealed that microglia dysfunction differed between patients with a *C9orf72* repeat expansion and patients with a mutation in progranulin, the latter accounting for 5-25% of familial FTD (31, 32). This suggests that the specificity of microglia dysfunction depends on the etiology of the patient population, and further emphasizes the need to better understand how microglia contribute to ALS and FTD. With respect to *C9orf72* ALS/FTD, it is notable that hallmark neuropathological features are most prominent in neurons compared to neighboring microglia (25, 33). However, no studies have addressed whether microglia dysfunction and the aberrant phenotypes they develop are intrinsic or evoked by a diseased cellular environment. It is also unknown whether microglia exhibit non-cell autonomous regulatory activities similar to what has been described for astrocytes and their ability to trigger motor neuron degeneration in ALS (9, 10, 34, 35).

Although several mouse models for *C9orf72* ALS/FTD have been generated, very little attention has been given to the specific role of microglia (36). While these mouse models display general microglia activation, the precise contribution of microglia to the observed phenotypes and pathologies remains unknown. Perhaps the most significant microglia phenotypes were observed in *C9orf72* knockout mice, which displayed signs of neuroinflammation and where microglia exhibited lysosomal accumulation and increased expression of pro-inflammatory cytokines including IL-6 and IL-1β (30, 37, 38). Furthermore, transcriptomic profiling revealed an upregulation of inflammatory pathways similar to what has been found in *C9orf72* FTD patient tissues (30, 39). Similarly, knocking out *C9orf72* with antisense oligonucleotides in mice led to the upregulation of *TREM2* and *C1qa,* which are both upregulated in activated microglia (40). In addition, a recent study showed that antibodies against one of the *C9orf72* DPR proteins, poly-(GA), reduced neuroinflammation in a poly-(GA) overexpressing mouse model (41). While limited, these *in vivo* studies support a role for microglia in *C9orf72* ALS/FTD pathogenesis.

In an effort to understand the contribution of non-neuronal cells to *C9orf72* ALS/FTD, we generated a human *in vitro* cell culture model by differentiating *C9orf72* ALS/FTD patient derived induced pluripotent stem cell (iPSCs) into microglia. While the use of a human iPSC-microglia (iPSC-MG) culture technique has only recently been developed, several studies have implemented this technology to study the role of microglia in neurodegenerative diseases, in particular Alzheimer's disease (42-48). To our knowledge, the intrinsic properties of microglia carrying a *C9orf72* HRE, and their role in *C9orf72* ALD/FTD neurodegeneration, have yet to be examined. Evaluations of human microglia seem particularly important since comprehensive studies on microglia single-cell expression patterns found that, while there is an evolutionary conserved gene core program, notable differences were uniquely found in primate microglia,

including complement, phagocytic and susceptibility genes to neurodegenerative diseases (49). This is supported by additional studies looking at human specific microglial gene expression changes in AD and Parkinson's disease (50-52).

Here, we generated iPSC-MG mono-cultures that express known microglia genes and proteins. These iPSC-MG also perform common microglia functions such as phagocytosis and the release of cytokines and chemokines upon exposure to extracellular stimuli. iPSC-MG generated from *C9orf72* ALS/FTD patients recapitulate aspects of *C9orf72* ALS/FTD pathology, but present with a virtually unaltered gene expression profile compared to control iPSC-MG based on RNA sequencing analyses. Nevertheless, *C9orf72* ALS/FTD iPSC-MG exhibit an altered inflammatory phenotype upon stimulation with lipopolysaccharide (LPS), and aberrant lysosomal accumulation following the phagocytosis of Aβ (1-40)-TAMRA protein or human brain synaptoneurosomes. These inflammatory phenotypes are accompanied by aberrant protein expression of early endosome antigen 1 (EEA1) and lysosomal associated membrane protein 1 (Lamp1). Of importance, microglia endosomal-lysosomal pathway dysfunction was similarly observed in the frontal cortex and motor cortex of *C9orf72* ALS/FTD patients. These studies provide the first thorough characterization of *C9orf72* ALS/FTD iPSC-MG mono-cultures and their intrinsic properties. These data further suggest that either or both a diseased environment and extracellular stimuli are critical to activate microglia and to initiate the disease-specific microglia phenotypes observed in postmortem patient brain tissues.

Methods

Generation of Hematopoietic Progenitor Cells (HPCs) DIV -1 to DIV 12

IPSCs were differentiated into microglia following an established protocol (53). Briefly, iPSCs were maintained in mTeSR Plus Kit (Stemcell Technologies # 05825) in 10cm dishes. At DIV -1 of HPCs differentiation, five to seven day old iPSCs cultures were then used to generate cluster of differentiating 43 positive ($CD43^+$) hematopoietic progenitor cells (HPCs) following a 12 day commercially available kit (STEMdiff Hematopoietic Kit; Stemcell Technologies # 05310). IPSCs were cleaned and 1/3 dish was gently dissociated with dispase (Stemcell Technologies # 07923) for 12-15 minutes at 37°C. IPSCs were then collected and spun down at 500rpm for 1-2 minutes and resuspended in 2mL of mTeSR Plus media with 20 μM ROCK inhibitor Y-27632 (Stemcell Technologies # 72304). Matrigel, hESC-Qualified Matrix (Corning # 354277) coated six well plates containing 2mL/well of mTeSR Plus media with 20 μM ROCK were used to start the HPC differentiation. Using a 5mL serological pipette, one drop or two drops of iPSCs were seeded per well. Then, next day, on DIV 0 of HPCs differentiation, wells with 80 small colonies per well were selected to start HPCs differentiation. IPSCs were fed following the manufacturer's instructions. On DIV 12 of HPCs differentiation, only the non-adherent HPCs were transferred to a new six well plate to start microglia differentiation (DIV 12/0).

Differentiation of HPCs into microglia cells DIV 12/0 – DIV 40/28

Matrigel, GFR (growth factor reduced) Membrane Matrix (Corning # 356231) coated six well plates were prepared to start microglia differentiation (DIV12/0). HPCs were differentiated into microglia for 28 days using serum free media conditions. HPCs in suspension were collected and spun down at 300 xG for 6 minutes and resuspended into microglia basal media (MBM, 2mL/well) containing: DMEM/F12 no phenol (Gibco # 11-039-021), 2% Insulin Transferin

Selenite (Gibco # 41400045), 2% B27 (Gibco # 17504-044), 0.5% N2 (Gibco # 17502-048), 1% Glutamax (Gibco # 35050-061), 1% NEAA (Gibco # 11140-050), 1% Pen/Strep (Gibco # 15140-122), 400µM 1-Thioglycerol (Sigma # M1753), 5µg/mL human insulin (Sigma # I2643) and supplemented with 3 growth factors (GFs): 100ng/mL human recombinant interleukin-34 (IL-34; Peprotech # 200-34), 25ng/mL macrophage colony-stimulating factor (M-CSF; Gibco # PHC9501) and 50ng/mL transforming growth factor β1 (TGFβ1; Miltenyi Biotec # 130-108-969) (MBM + 3GFs); cytokines and growth factors known to be essential for the development of microglia (54-61). Microglia differentiation starts (DIV 12/0) once the HPCs are transferred and plated at a density of 200 000 cells per well of a six well. Cells will predominantly grow in suspension. On DIV 2, 4, 6, 8 and 10 of microglia differentiation, 1mL of MBM + 3GFs media was added to each well. On DIV 12, a partial media change was done. IPSC-MGs from one six well plate were spun down at 300 xG for 6 minutes and resuspended into MBM + 3 GFs and split back into the same six well plate. On DIV 14, 16, 18, 20, 22, 24, 1mL media was added per well. On DIV 25, MBM + 3GFs was changed to maturation media composed of MBM supplemented with the 5 growth factors (MBM +5 GFs): 100ng/mL IL34, 25ng/mL M-CSF and 50ng/ml TGFβ1, 100ng/mL cluster of differentiation 200 (CD200; Novoprotein # C31150UG) and100ng/mL fracktaline chemokine C-X3-C motif ligand 1 (CX3CL1; Peprotech # 300-31) (MBM + 5 GFs). The presence of CD200 and CX3CL1 in the culture media, both glial and neuronal molecules are critical for microglia maturation and maintenance of an *in vivo*-like microglia resting state phenotype in an *in vitro* setting (62-64) (Fig. 1a). At DIV 28, IPSC-MG reached maturation. 1mL of MBM + 5GFs media was added to the cultures every other day. Mature cells were used for experimentation within 10 days (DIV 28-DIV38).

Differentiation of iPSCs into cortical neurons

For cortical neuron differentiation, 70% confluent iPS cells maintained in mTeSR Plus media on 10 cm dishes were used for embryoid bodies (EBs) formation. The cells were cultured in low attachment six well plates (Greiner bio-one # 657970) using WiCell Medium containing: DMEM/F12 (Gibco #11330057), 25% knock out serum replacement (Gibco # 10828-028), 1.3% L-glutamine (Gibco # 35050-061), 1.3% NEAA (Gibco # 11140-050), 0.1mM 2-Mercaptoethanol (Sigma# M3148) and placed on a shaker in the incubator for 8 days to allow EBs formation. EBs were then resuspended in Forebrain Neural Induction Media (FB-NIM) containing: DMEM/F12, 1% N2 supplement (Gibco # 17502-048), 1% NEAA, 2ug/mL heparin (Sigma # H3149), 10 µg/mL bFGF (Stemcell Technologies # 78003) and plated on to T25 flasks coated with basement membrane matrigel (Corning # 356234) to allow formation of neuronal rosettes. Neuronal rosettes were maintained in FB-NIM for the next 10 days and then, collected and maintained in suspension on a shaker with half FB-NIM media changes every other day to allow for neurosphere growth. Neurospheres were maintained for 20 days in FB-NIM and then resuspended using forebrain neuronal differentiation media (FB-DM) containing: Neurobasal Medium (Corning # 21103-049), 2% B27 (Gibco # 17504-044), 10 ug/mL BDNF (Stem cell technologies # 78005), 10 ug/mL GDNF (Stem cell technologies # 78058), 1µg/mL laminin (Life technologies # 23017-015), 3.3 µg/mL cAMP (Stem cell technologies # 73884), 3.52 µg/mL Ascorbic acid (Stem cell technologies # 72132), 0.5mM L-glutamine and 1% NEAA and then plated on to T25 flasks. iPSC cortical neurons were harvested on DIV 65-72 for RNA sequencing analysis.

Immunocytochemistry of iPSC-MG

For iPSC-MG DIV 28-33 of microglia differentiation, non-adherent iPSC-MGs were collected and plated onto a 4 or 8 well fibronectin (sigma # F0895; 1:40) coated chamber slides at a seeding density of 250 000 or 125 000 cells per well respectively. One hour after plating, cells were fixed with 4% paraformaldehyde (PFA; Electron Microscopy Sciences # 15714-S) for 20 minutes, washed three times in PBS for 5 minutes and then, blocked with 0.2% Triton X-100 and 5% Normal Goat Serum (Vector # S1000) for 1 h at room temperature. Primary antibodies were prepared in blocking solution and applied overnight at 4 °C. The following primary antibodies were used during our studies: anti- PU.1 (Cell Signaling Technology # 2266S) 1:500; anti-P2RY12 (Sigma # HPA014518) 1:500; anti-CX3CR1 (Biorad/AbD Serotec # AHP1589) 1:500; anti-TREM2 (abcam # AB209814) 1:500; anti-TMEM119 (abcam # ab185333) 1:100; anti-LAMP1 (Developmental Hybridoma Bank # H4A3-s) 1:100; anti-EAA1 (BD Biosciences # 610457) 1:700; anti-C9orf72 (Sigma # HPA023873) 1:100; anti-TDP-43 (Cell signaling # 89789, TDP-43 D9R3L) 1:500; anti-ADAR-2 (Sigma # HPA018277)1:500. Next, cells were washed in PBS three times for 7 min and then, incubated consecutively with respective fluorophores secondary antibodies. Alexa Fluorophores (Invitrogen) were used at a 1:750 and prepared in blocking solution without triton and incubated for 45 minutes at room temperature. Cells were then washed with PBS three times for 7 min each and DAPI was applied. For nuclear markers TDP-43 and ADAR, wheat germ agglutinin 680 (Invitrogen # W32465) was used to label iPSC-MG cell surface. Mounting media ibidi (ibidi # 50001) was used on chambers slides.

RNA isolation, whole transcriptome library preparation, and sequencing

At DIV 28-30 iPSC-MG from 7 *C9orf72* ALS/FTD patient lines and 4 control lines were pelleted and lysed using QIAshredder (QIAGEN-79654) and RNA was isolated with RNeasy Mini Kit (QIAGEN-74104) following the manufacturer's instructions. RNA samples were measured for quantity with Quant-iT Ribogreen RNA Assay (Thermo Fisher, Cat. No. R11490) and quality with Agilent High Sensitivity RNA ScreenTape and buffer (Agilent, Cat. No. 5067-5579 & 5067-5580). For each RNA sample, an indexed, Illumina-compatible, double-stranded cDNA whole transcriptome library was synthesized from 1μg of total RNA with Takara Bio's SMARTer Stranded Total RNA Sample Prep Kit – HI Mammalian (Takara Bio, Cat. No. 634876) and SMARTer RNA Unique Dual Index Kit (Takara Bio, Cat. No. 634418). Library preparation included ribosomal RNA depletion, RNA fragmentation (94 °C for 3 min), cDNA synthesis, and a 12-cycle unique dual indexing enrichment PCR. Each library was measured for size with Agilent's High Sensitivity D1000 ScreenTape and reagents (Agilent, Cat. No. 5067-5584 & 5067-5603) and concentration with KAPA SYBR FAST Universal qPCR Kit (Kapa Biosystems, Cat. No. KK4824). Libraries were then combined into an equimolar pool which was also measured for size and concentration. The pool was clustered onto a paired-end flowcell (Illumina, Cat. No. 20012861) with a 20% v/v PhiX Control v3 spike-in (Illumina, Cat. No. FC-110-3001) and sequenced on Illumina's NovaSeq 6000. The first and second reads were each 100 bases.

Human tissue RNA sequencing

We accessed human brain tissue RNA sequencing performed by Target ALS and the New York Genome Center (http://www.targetals.org/research/resources-for-scientists/resource-genomic-

data-sets/). Sixteen cases of control frontal cortex, 8 *C9orf72* ALS/FTD frontal cortex, 15 control motor cortex, 12 *C9orf72* ALS/FTD frontal cortex, 4 control occipital cortex and 5 *C9orf72* ALS/FTD frontal cortex were evaluated for differential expression of microglia specific genes (Table S4). All sequencing data is publicly available at https://metronome.nygenome.org/tutorials/.

RNA sequencing analysis

Fastq files were quality and adapter trimmed using cutadapt (version 1.14). Adapter trimmed fastq files were then aligned to the human genome (hg38, gencode v29) using STAR (version 2.6.1d) with default options. RNA count matrices were pulled from aligned BAM files using featureCounts (version 1.6.4). All downstream statistical analysis was done in R (version 3.6.2) using raw counts matrices from featureCounts as input. Low expression genes were filtered such that genes with mean read counts < 10 were removed from the analysis. Differential expression analysis was done using DESeq2 (version 1.26.0) using disease status as the model. Volcano plots were generated from DESeq2 output using EnhancedVolcano. Heatmaps were generated using heatmap from z-scores calculated from DESeq2 normalized gene counts. Tissue data from Target ALS was downloaded from the New York Genome Center as raw fastq files and pushed through an identical analysis pipeline as data generated in our lab.

Repeat primed PCR to detect the presence of C9 HRE in iPSC and iPSC-MG

We followed previous established protocols (65) to determine the presence the hexanucleotide repeat expansion (G_4C_2: >30) in *C9orf72* of iPSC and iPSC-MG (Table S2).

Real-time quantitative RT-PCR

RNA was isolated using Qiagen RNeasy Micro Kit (Cat #74004) according to manufacturer's instructions. RNA was reverse transcribed to cDNA with oligo(dT) with the Promega Reverse Transcriptase System (Cat # A3500) and analyzed using SYBR Green Master Mix (Applied Biosystems). *C9orf72* (Forward- 5'- CAGTGATGTCGACTCTTTG -3' and Reverse- 5' AGTAGCTGCTAATAAAGGTGATTTG -3'). Expression was normalized to RPL13A (Forward- 5' CCTGGAGGAGAAGAGGAAAGAGA-3' and Reverse- 5' TTGAGGACCTCTGTGTATTTGTCAA-3') or B2M (Forward- 5' TGCTGTCTCCATGTTTGATGTATCT-3' and Reverse- 5' TCTCTGCTCCCCACCTCTAAGT-3').

Western blotting

Microglia cell pellets were homogenized in RIPA lysis and extraction buffer (Thermo Scientific, Cat #89900), supplemented with protease inhibitor cocktail (complete, Roche) and phosphatase inhibitor cocktail (PhosSTOP, Roche). Protein concentration was determined by BCA assay kit (Thermo Fisher, Cat# 23225). Cell lysates were separated on 4-20% protean TGX precast gels (Biorad, Cat # #4561096) and blotted onto nitrocellulose membranes (Biorad, Cat # 1704159). Membranes were blocked for 60 min with Odyssey blocking buffer (PBS, Li-Cor, Cat #927-40000) and incubated overnight at 4°C with anti-C9orf72 (GeneTex Cat #. GTX634482, 1:1000), and anti-β tubulin (Sigma-Aldrich T6074, 1:1000) antibodies. After washing membranes were

incubated for 60 min with IRDye fluorescent secondary antibodies (Li-Cor). After washing, blots were subsequently analyzed with Li-COR imaging system (Odyssey CLx).

Immunoassay analysis of poly-(GP)

Levels of poly-(GP) in cell lysates were measured in a blinded fashion using a Meso Scale Discovery (MSD) immunoassay and a MSD QUICKPLEX SQ120 instrument. A purified mouse monoclonal poly-(GP) antibody was used as both the capture and detection antibody (TALS 828.179, Target ALS Foundation). The capture antibody was biotinylated and used to coat 96-well MSD Small Spot Streptavidin plates, whereas the detection antibody was tagged with an electrochemiluminescent label (MSD GOLD SULFO-TAG). Lysates were diluted to the same protein concentration, and each sample was tested in duplicate. For each well, the intensity of emitted light, which is reflective of poly-(GP) levels and presented as arbitrary units, was acquired upon electrochemical stimulation of the plates.

Phagocytosis of Aβ protein by iPSC-MG

On DIV 30 of microglia differentiation, iPSC-MGs were plated on to 4 chambers glass slides coated with human fibronectin (sigma # F0895; 1:40) at a cell density of 250 000 cells per chamber. One hour after plating, iPSC-MGs were treated for 5 minutes with vehicle (DMSO) or 1μM of fluorescently labeled Aβ (1-40) TAMRA (human Aβ, AnaSpec # AS-60488; (66)) prepared in microglia basal media with growth factors. All iPSC-MGs were washed at 5min with microglia basal media supplemented with growth factors. IPSC-MGs were then fixed after 5 minutes, 30 minutes, and 1 h and immunostained for TREM2 as described above. Cells were

then imaged using a Zeiss LSM800 confocal microscope. Using Imaris Software from Bitplane we determine the cell volume and percentage of the microglia surface area covered by Aβ (1-40) TAMRA at different time points.

Generation of human brain synaptoneurosomes

Fluorescently labeled pHrodo (a pH sensitive dye that fluoresces only in acidic compartments) human brain synaptoneurosomes (hSN-rodo) were generated as described previously (67, 68). Briefly, brain tissue from temporal cortex people with no neurological disease was acquired from the MRC Edinburgh Sudden Death Brain Bank. Use of human tissue for post-mortem studies has been reviewed and approved by the Edinburgh Brain Bank ethics committee and the ACCORD medical research ethics committee, AMREC (approval number 15-HV-016; ACCORD is the Academic and Clinical Central Office for Research and Development, a joint office of the University of Edinburgh and NHS Lothian). The Edinburgh Brain Bank is a Medical Research Council funded facility with research ethics committee (REC) approval (11/ES/0022). Frozen tissue was homogenized in buffer containing 25mM HEPES, 120 mM NaCl, 1 mM $MgCl_2$, 2 mM $CaCl_2$, and protease and phosphatase inhibitors. The homogenate was passed through an 80 μm filter then a 5 μm filter then centrifuged at 1000xg for 7 minutes to yield the synaptoneurosome pellet. Pellets were resuspended in 100 mM sodium carbonate buffer (pH 9) and tagged with pHrodo Red at 4mg/mL with gentle shaking at room temp for 1 hour. Samples were centrifuged at 13,000 rpm for 10 minutes and the pellet containing labelled synaptoneurosomes was washed 3x with PBS to remove unbound dye and resuspended in 5% DMSO-PBS.

Engulfment of human brain synaptoneurosomes by iPSC-MG

On DIV 30 of the microglia differentiation, iPSC-MGs were plated on to 8 chamber glass slides that were coated with human fibronectin (sigma # F0895; 1:40) at a cell density of 62 000 cells per chamber. One hour after plating, we labeled live microglia with the nuclear marker Hoechst 33342 (Thermo fisher # H3570). Then, control and *C9orf72* iPSC-MGs were treated with 1:100 dilution of 4mg/mL hSN-rodo in the presence or absence of 10 μM cytochalasin-D (inhibitor of actin polymerization). Confocal live cell imaging of iPSC-MGs was done using a 20X objective of a Zeiss 800 confocal microscope. IPSC-MGs were imaged every 10 minutes for up to 6 h. All lines had three technical replicates for the hSN-rodo treatment. Six images were taken per well of each line for a total of 18 images every 10 minutes. All images were analyzed using Imaris Software from Bitplane. To determine the percentage of iPSC-MGs engulfing hSN-rodo, the spots module was used to count the total number of iPSC-MGs and the total number of phagocytic iPSC-MGs per image. Additionally, we quantified the fluorescence mean intensity of the cargo hSN-rodo per phagocytic cell at the 2 h time point, where more than 60% of the iPSC-MGs were engulfing hSN-rodo. Cytochalasin D was used as a negative control.

Immunofluorescence of human tissue

Cognitive impaired *C9orf72* positive and non-ALS control patient postmortem frontal cortex and motor cortex tissue were obtained from Target ALS (n= 2 cases per group, Table S5). Paraffin embedded sections were de-paraffinized in two separate 10 minute Clearite (Thermo Fisher # 6901) washes. Sections were dehydrated in subsequent two 100%, one 95%, and one 70%

ethanol 3 minute washes. Sections were then washed three times in PBS for 5 minutes each. Antigen retrieval was then performed in 10 mM Na-Citrate buffer (pH 6.0) for 10 minutes in a microwave at 80% power. Slides were cooled at room temperature for 1 h, then washed in PBS three times for 5 minutes each. Sectioned tissue was blocked at room temperature for 1 h in Dako blocking solution (Dako # X0909). Sections were then incubated in antibody dilutant (Dako # S3022) solution containing primary antibodies anti-Iba1 (Wako # 019-19741) at 1:500 and either EEA1 (BD Biosciences # 610457) at 1:50 or LAMP1 (DSHB # H4A3) at 1:50 for 16 h at 4°C in a humidified chamber. Human sections were washed three times for 10 minutes each in PBS then incubated in Dako antibody dilutant with 1:500 Alexa Fluor 488 (Invitrogen # A11029) secondary antibody for 1 h at room temperature. The tissue sections were then washed three times in PBS for 10 minutes. This was followed by incubation in Dako antibody dilutant solution containing 1:500 Alexa Fluor 555 (Invitrogen – A21429) secondary antibody for 1 h at room temperature. Again, the tissue sections were washed three times in PBS for 10 minutes each. Finally, the sections were incubated in DAPI (Invitrogen # D1306) 1:10,000 in PBS for 15 minutes, and then washed once more for 5 minutes in PBS. The sections were coverslip using ProLong™ Glass Antifade Mountant (Invitrogen # P36984).

IPSC-MG cytokine assay

On DIV 29, iPSC-MGs were plated on to 4 chambers glass slides coated with human fibronectin (sigma # F0895; 1:40) at a cell density of 250 000 cells per chamber. On DIV 30, control and disease iPSC-MGs were treated with LPS (100ng/mL) for 6 h, based on previous studies (69,

70). The conditioned media was collected and analyzed for cytokine/chemokine profile using the V-PLEX human cytokine kit (Mesoscale) per manufacturer's protocol.

Confocal microscopy and bright-field imaging

All immunostained iPSC-MGs and *post-mortem* human tissue were visualized and imaged using a Zeiss LSM800 laser scanning confocal microscope. Per staining, all images were taken with same settings for parallel cultures. For all iPSC-MG immunostainings and Aβ (1-40) TAMRA phagocytic activity assay, a plan Apochromat 63x oil immersion objective was used; Z-stacks were generated with 1024 x 1024 image size, 0.5x XY scan zoom and 1μm scaling. For some immunostainings, differential interference contrast (DIC) was used to highlight iPSC-MG surface area. For live cell imaging of iPSC-MG engulfing synaptoneurosomes, confocal microscopy with differential interference contrast was used. Tiled images were captured using a 20X objective with a 1.0x XY scan zoom and 0.624 μm x 0.624μm scaling. For human tissue staining, all tissue sections were imaged using Plan Apochromat 63x oil immersion objective with a 2x zoom. Z-Stack images were acquired using identical laser settings and normalized within a given experiment. Bright-field images of the iPSC-MG cultures were taken using a Zeiss AxioVert.A1 microscope and a resolve HD Ludesco camera.

Imaging analysis using Imaris Software from Bitplane

All images were processed and analyzed using Imaris Software 9.5.1 and 9.6 from Bitplane. In order to obtain volume, area, mean intensity and sum intensity per cell for a large number of samples, we assigned a randomized color identification per cell followed by the use of

ImarisVantage module to extract multiple numerical values from the created 3 dimensional structures. For *iPSC-MG marker characterization*, the spots module was used to count the total number of cells positive for a specific microglia marker per image while using the DAPI channel as a reference. To calculate the *TDP-43 and ADAR-2 nucleocytoplasmic ratio (N/C ratio),* we used the surface module to generate iPSC-MG microglia 3 dimensional cellular (based on membrane staining with wheat germ agglutinin) and nuclear surfaces (based on DAPI). The sum intensity of TDP-43 or ADAR-2 was acquired for the nucleus and cytoplasm as well as the volume for each cellular compartment. The following formula was used: (Cell Sum Intensity – Nucleus Sum Intensity) = Cytoplasm Sum Intensity; (Cell Volume – Nucleus Volume) = Cytoplasm Volume. *N/C ratio* = (Nucleus Sum Intensity/ Nucleus volume) / (Cytoplasm Sum Intensity/ Cytoplasm volume). Data from each cell was acquired by assigning randomized color identification followed by the use of ImarisVantage. For the *Aβ (1-40) TAMRA phagocytic activity*, we used *Aβ (1-40) TAMRA* fluorescence signal and chose an ideal threshold to create the *Aβ* surfaces inside the IPSC-MGs. TREM2 staining was used to generate the cell surface structures. An algorithm was also generated and used in all iPSC-MG parallel cultures. Randomized color identification and ImarisVantage was also used to extract all data like previous data sets. For *hSN-rodo live cell imaging over time,* the spots module was used to count the total number of cells over time. Phagocytic cells were manually identified based on hSN-rodo signal inside iPSC-MG per hour. We set a threshold between 10,000-12,000 units above grey scale as the positive signal indicative of engulfment and lysosomal internalization. At the 2 h time point, the cell surface area of phagocytic cells was manually outlined using Imaris Software manual creation tool and the hSN-rodo mean intensity value was obtained per cell. For

iPSC-MGs EEA1 and Lamp1 analysis, based on the staining pattern we manually choose an optimal threshold for each protein marker to generate the 3D surfaces. We then, stored the surfaces algorithms and used it in all iPSC-MG parallel cultures. Randomized color identification and ImarisVantage were then used to extract the cell volume and mean intensity of both markers per cell. For *EEA1 and Lamp1 post-mortem human tissue analysis (Frontal cortex and Motor cortex),* microglia 3 dimensional cell surface was generated per image and the mean intensity of each cytoplasmic marker was quantified per cell.

Statistical analysis

Statistical Analysis for RNA sequencing was done in R (version 3.6.2) and detailed above. All other statistical analyses were performed using Graphpad Prism 7 and 8. For comparison of two groups we used two-tailed Student's t-test. Two tailed Mann Whitney test was performed for the poly-(GP) ELISA assay. We performed multiple t-test for the iPSC-MGs cytokine release profile, to adjust for multiple corrections we used Holm-Sidak method. All statistical significance was ranked as the following: * $p \leq 0.05$; ** $p \leq 0.01$; *** $p \leq 0.001$; **** $p \leq 0.0001$ and $p > 0.05$ not significant. All other statistical details and exact p-values are reported in each Figure legend.

Results

C9orf72 ALS/FTD patient and control iPSCs differentiate into brain-like microglia

Following recently established protocols (53, 57) we differentiated control and *C9orf72* ALS/FTD patient iPSC lines into microglia (Fig. 1a; Additional File 7: Table S1-S3). At a mature stage of 40 days *in vitro* (DIV), both control and *C9orf72* ALS/FTD iPSC-MG display a typical ramified

microglia morphology (Fig. 1b) and express classic microglia marker proteins including the myeloid transcription factor PU.1, purinergic surface receptor P2RY12 and C-X3-C Motif Chemokine Receptor 1 (CX3CR1), as confirmed via fluorescent immunocytochemistry (Fig. 1c; Additional File 1: Figure S1a-b). Differentiated microglia uniformly expressed the triggering receptor expressed on myeloid cells 2 (TREM2) and transmembrane protein 119 (TMEM119), further demonstrating a commitment to microglia fate, with no differences detected between *C9orf72* iPSC-MG and control iPSC-MG (Fig. 1c; Additional File 1: Figure S1a-b). To validate microglia lineage, we performed Illumina paired-end deep RNA sequencing analysis (RNA-seq) on control and *C9orf72* ALS/FTD iPSC-MG (Fig. 1d-e). At a transcriptional level, control and *C9orf72* iPSC-MG clustered together and presented with a unique transcriptome compared to iPSC differentiated into cortical neurons (iPSC-CN; Fig. 1d). Principal component analysis of this RNA-seq dataset revealed a highly similar gene expression profile within iPSC-MG and different from iPSC-CNs (PC2, 1.66% variance), confirming that these populations are distinct from each other (PC1, 94.87% variance; Fig. 1e). Moreover, to verify the absence of other cell types in the differentiated iPSC-MG cultures, we quantified known cell type specific markers revealing high expression of microglia-enriched genes and low expression for transcripts unique to astrocytes, oligodendrocyte precursor cells (OPC), oligodendrocytes, neurons, endothelial cells and pericytes (71) (Fig. 1f). These data confirm that the differentiation of microglia from iPSC results in brain-like microglia that express microglia-enriched genes and proteins, distinct from other cell types. Furthermore, no inherent differences were observed between control and *C9orf72* ALS/FTD iPSC-MGs.

The transcriptional profile of C9orf72 ALS/FTD iPSC-MG resembles control iPSC-MG

To test if *C9orf72* microglia exhibit intrinsic disease-mediated gene expression alterations, we analyzed our RNA sequencing data for differential expression between mature control and *C9orf72* ALS/FTD iPSC-MG. This analysis revealed several genes with significantly altered expression in *C9orf72* ALS/FTD iPSC-MG (27 genes; log_2 fold change (FC) ± 1, p value <0.05; Fig. 2a; Additional File 2: Figure S2a). We next determined if 881 RNA transcripts previously reported to be enriched in cortical microglia were differentially expressed in our dataset, but found no significant dysregulation of these select genes (Fig. 2b) (52). These data suggest that the *C9orf72* HRE does not alter the inherent microglia-enriched transcriptional profile indicating that *C9orf72* ALS/FTD and control iPSC-MG share a similar transcriptome in the absence of surrounding CNS cell types, including neurons and macroglia, such as astrocytes and oligodendrocytes. To support this hypothesis we analyzed existing RNA sequencing datasets obtained through the Target ALS consortium and the New York Genome Center. We evaluated gene expression changes of the 881 microglia-enriched RNA transcripts in frontal cortex and motor cortex brain tissues of *C9orf72* ALS/FTD patients (Fig. 2c-d; Additional File 2: Figure S2b; Additional File 7: Table S4). We also quantified gene expression changes in the occipital cortex as a brain region considered to be disease-unaffected in ALS/FTD (Additional File 2: Figure S2c-d; Additional File 2: Table S4). Notably, of the 881 microglia-enriched genes, 18 were dysregulated in frontal cortex, 20 in motor cortex and eight in the occipital cortex (Fig. 2c-d; Additional File 2: Figure S2b-d). It is important to note that gene expression alterations in diseased microglia would not only consist of microglia-enriched transcripts, but also transcripts critical for cellular health and function expressed in all cell types. However, these were not

captured through the analysis of the 881 microglia-enriched genes. Therefore, we expanded our analysis of the RNA-seq dataset to examine overall transcriptional changes in the select brain regions, not cell-type specific, which revealed significant gene dysregulations in all brain regions of *C9orf72* ALS/FTD brain tissues (Additional File 3: Figure S3a-b; (log_2 fold change (FC) ± 1, p value <0.05). Together these data suggest that the *C9orf72* HRE in iPSC-MG mono-cultures is not sufficient to induce inherent transcriptional alterations of microglia-enriched genes.

C9orf72 ALS/FTD iPSC-MG exhibit reduced C9orf72 protein levels and express C9orf72 hexanucleotide repeat expansion-associated poly-(GP) DPR protein

The study of ALS and FTD has long taken a neurocentric approach, whereby neurons have traditionally been recognized as the cell type most affected by the aforementioned *C9orf72* disease mechanisms. However, glia cells have been shown to exhibit *C9orf72* associated phenotypes in postmortem tissue, including repeat RNA foci and DPR proteins, albeit to a lesser extent than neurons (33, 72-76).

To evaluate *C9orf72* iPSC-MG for *C9orf72*-specific disease mechanisms, we first tested *C9orf72* iPSC-MGs for haploinsufficiency by examining the levels of the *C9orf72* transcript in *C9orf72* ALS/FTD and control iPSC-MG. Many studies have reported *C9orf72* haploinsufficiency in patient tissue, however variable results have been observed in human patient-derived *C9orf72* iPSC-differentiated cells, including neurons and astrocytes (72, 76, 77). In a similar fashion, no differences in *C9orf72* transcript levels were detected between control and *C9orf72* iPSC-MG in our RNA-seq dataset (Fig. 3a) or by quantitative RT-PCR of *C9orf72* (Fig. 3b), which is consistent with previous published data. To measure C9orf72 protein levels we performed

quantitative western blot analysis from control and *C9orf72* ALS/FTD iPSC-MG lysates, which revealed a significant reduction in C9orf72 protein in *C9orf72* ALS/FTD iPSC-MGs (Fig. 3c-d; Additional File 4: Figure S4a). The western blot analysis was further confirmed by C9orf72 immunostaining of iPSC-MG (Fig. 3e).

Sense and antisense GGGGCC/CCCCGG repeat associated non-AUG (RAN) translation produces five different DPR proteins that accumulate in cells and are proposed to contribute to toxicity and cellular dysfunction (78-83). Here, we assessed the presence of poly-(GP) in mature iPSC-MG cultures by measuring poly-(GP) abundance in cell lysates using a customized immunoassay (84). We detected a significant increase in poly-(GP) levels in *C9orf72* ALS/FTD iPSC-MGs compared to controls, showing for the first time that the *C9orf72* HRE translates into DPR proteins in microglia mono-cultures (Fig. 3f).

Cytoplasmic TDP-43 inclusions are the hallmark pathology of ALS and FTD and have been reported in glia cells of *C9orf72* ALS/FTD postmortem tissues (85-87). To evaluate whether iPSC-MG mono-cultures exhibit cytoplasmic TDP-43 inclusions, we performed immunocytochemistry on iPSC-MG for TDP-43 and measured the nucleocytoplasmic (N/C) ratio of TDP-43 using confocal microscopy. No significant difference in the TDP-43 N/C ratio was observed between control and *C9orf72* ALS/FTD microglia at 40 DIV (Additional File 4: Figure S4b-c). One explanation for TDP-43 mislocalization is a defect in nucleocytoplasmic trafficking leading to the retention of TDP-43 protein in the cytoplasm (88-90). Our laboratory has recently shown that another RNA binding protein, the RNA editing enzyme adenosine deaminase acting on double stranded RNA 2 (ADAR2), is mislocalized to and accumulates in the cytoplasm of neurons in *C9orf72* ALS/FTD (91). We therefore wondered whether *C9orf72* microglia would

display ADAR2 mislocalization despite the lack of cytoplasmic TDP-43 inclusions. Similar to TDP-43, immunocytochemistry of *C9orf72* ALS/FTD iPSC-MG for ADAR2 revealed no nucleocytoplasmic mislocalization resulting and an unchanged N/C ratio in microglia mono-cultures (Additional File 4: Figure S4d-e). These data suggest that, while *C9orf72* ALS/FTD iPSC-MG mono-cultures do exhibit *C9orf72* pathobiological phenotypes, there are no microglia cytoplasmic inclusions of TDP-43 or ADAR2, unlike what is seen in *C9orf72* neurons.

C9orf72 ALS/FTD iPSC-MG present with a pro-inflammatory phenotype

Microglia are able to exacerbate or promote neurodegeneration by releasing pro-inflammatory cytokines, including interleukin-1 (IL-1), interleukin-6 (IL-6) and tumor necrosis factor-α (TNF-α), or anti-inflammatory cytokines such as interleukin-4 (IL-4) and interleukin-10 (IL-10) (92-94). As a result, neuroinflammation is considered a major contributor to neuronal dysfunction in neurodegenerative diseases, including ALS/FTD (24, 94-96). To investigate if *C9orf72* ALS/FTD iPSC-MG respond differently to extracellular stimuli, we treated iPSC-MGs with LPS, an endotoxin used to evoke immune responses *in vitro* and *in vivo*. Following LPS treatment, we tested for the presence of released chemokines and cytokines in the iPSC-MG cell culture supernatants, as described recently (57). Under basal conditions, *C9orf72* ALS/FTD iPSC-MG mono-cultures showed a significant increase in IL-1α, IL-6 and TNF-α compared to control iPSC-MGs (Fig. 4). Upon LPS stimulation, both control and *C9orf72* ALS/FTD iPSC-MG exhibited increased release of IL-1α, IL-1β and IL-6 compared to basal conditions, with a significantly higher increase detected in *C9orf72* iPSC-MGs (Fig. 4). These results confirm the ability of iPSC-

MG to respond to extracellular stimuli via specific cell surface receptor activation and support previous studies showing altered pro-inflammatory responses of *C9orf72* microglia (30).

C9orf72 ALS/FTD iPSC-MGs exhibit altered phagocytic activity

A major function of microglia is to clear unwanted toxic substances and cell debris that can negatively impact brain function via phagocytosis. To determine whether control and *C9orf72* ALS/FTD iPSC-MG differ in their phagocytic activity and ability to clear toxic products we measured iPSC-MG engulfment of a fluorescently tagged Aβ cargo, known to be phagocytosed by microglia (66, 97). We treated iPSC-MGs for 5 minutes with 1μM Aβ (1-40)-TAMRA or vehicle and then assessed engulfment and clearance of Aβ (1-40)-TAMRA at different time points after Aβ washout. To quantify this engulfment, we performed immunohistochemistry on iPSC-MG for TREM2, an immune receptor selectively expressed in microglia (Fig. 5 a-c; g-i). We then calculated the percentage of iPSC-MG surface area covered by Aβ (1-40)-TAMRA protein in individual cells (Fig. 5 d-f; Fig. 5j-l). Aβ (1-40)-TAMRA was similarly internalized in both experimental groups after 5 minutes suggesting a comparable degree of uptake between control and *C9orf72* iPSC-MG (Fig. 5m). However, after 30 minutes and 1 h, *C9orf72* ALS/FTD iPSC-MG exhibited increased cellular Aβ (1-40)-TAMRA loading suggesting delayed clearance of engulfed Aβ (1-40)-TAMRA from intracellular compartments compared to control iPSC-MG (Fig. 5m). No significant differences in the total microglia cell surface area were observed (Fig. 5n). These data suggest that the mutation in *C9orf72* alters protein degradation pathways in iPSC-MG.

C9orf72 ALS/FTD iPSC-MGs demonstrate altered engulfment of human brain synaptoneurosomes

An important aspect of microglia-neuron communication in neurodegeneration is the role of microglia in the maintenance and refinement of synaptic networks through the selective pruning of synapses. This process occurs predominantly, but not exclusively, during development (98-100). However, synaptic pruning pathways are known to be re-activated in neurodegeneration leading to synapse loss and contributing to cognitive impairments (101-104). To determine if iPSC-MG can phagocytose synapses and to test whether *C9orf72* microglia exhibit altered phagocytosis due to the *C9orf72* HRE, we exposed iPSC-MG mono-cultures to human brain synaptoneurosomes (hSN) and followed synaptoneurosomes engulfment via live confocal microscopy. Fresh frozen control human postmortem tissues were used to prepare hSN. Synaptic fractions contained the pre-synaptic protein synaptophysin and the post-synaptic density 95 (PSD-95) compared to total brain homogenate and nuclear marker histone 3 (Additional File 5: Figure S5a-b). Control and *C9orf72* ALS/FTD iPSC-MGs were labeled with the live nuclear marker Hoechst (Fig. 6a-i) to identify individual cells followed by treatment with hSN fluorescently tagged with pHrodo succinimidyl ester (hSN-rodo; Fig. 6a; Fig. 6j-q). After treatment of iPSC-MGs with hSN-rodo we performed fluorescent live cell imaging for 6 h, capturing images every 10 min (Additional File 6: Figure S6 and Additional File 8: Movie S1). Here, an increase in pHrodo fluorescence is indicative of an uptake of hSN-rodo into acidic intracellular compartments of iPSC-MGs. Quantification of individual iPSC-MG showed a distinct rapid internalization of hSN-rodo in control and *C9orf72* ALS/FTD iPSC-MGs (Fig. 6r). iPSC-MG phagocytosis was reduced significantly in the presence of cytochalasin-D, an actin

polymerization inhibitor known to inhibit phagocytosis (Fig. 6r-s). 69% of control and 71% of *C9orf72* iPSC-MG were actively phagocytosing after 2 h (Fig. 6r). Interestingly, the mean intensity of hSN-rodo was significantly increased in *C9orf72* ALS/FTD iPSC-MGs compared to controls (Fig. 6s). Together, these data suggest that iPSC-MG exhibit known microglia phagocytic activity as shown by the engulfment of toxic Aβ protein and brain synaptoneurosomes. Moreover, *C9orf72* ALS/FTD iPSC-MGs displayed increased levels of phagocytosed synaptoneurosomes, which can be explained through increased phagocytic activity or insufficient degradation of engulfed content, reflecting the data from the Aβ uptake studies above.

C9orf72 ALS/FTD iPSC-MG exhibit aberrant levels of EEA1 and Lamp1

The major function of the C9orf72 protein is the regulation of vesicle trafficking. The C9orf72 protein structure resembles that of a Rab guanine nucleotide exchange factor (RabGEF), which in turn activates Rab proteins to regulate membrane trafficking (105, 106). Supporting this notion is evidence of C9orf72 protein expression in endosomes, autophagosomes and lysosomes and the fact that *C9orf72* KO mice display defects in the endosomal/lysosomal pathway, as well as dysregulation of autophagy (30, 107, 108). Studies of the motor cortex and spinal cord of *C9orf72* ALS/FTD postmortem tissues showed enlarged lysosomes in activated microglia suggesting that endosomal/lysosomal dysfunction could also be affected in this cell type due to the *C9orf72* HRE (30, 108, 109).

Based on these studies, and our observations of increased retention of phagocytosed extracellular products in *C9orf72* ALS/FTD iPSC-MG described above, we performed

immunohistochemistry for early endosomal and lysosomal markers in control and *C9orf72* ALS/FTD iPSC-MG. Using confocal microscopy images we generated 3D surfaces of control (Fig. 7a,d,g) and *C9orf72* ALS/FTD iPSC-MG (Fig. 7b,e,h) to quantify changes in protein expression of EEA1 (Fig. 7c) and Lamp1 (Fig. 7f), and to measure microglia cell surface volume (Fig. 7i). While no significant changes were observed in iPSC-MGs cell volume (Fig. 7i), quantification of the mean fluorescence intensity of EEA1 and Lamp1 per cell revealed a significant increase in EEA1 (Fig. 7a-c) and a significant reduction in Lamp1 (Fig. 7d-f). We found no significant differences in the relative expression of mRNA in the endosomal-lysosomal pathway (Fig. 7j). Overall, these data suggest that the mutation in *C9orf72* alters the endosomal-lysosomal pathway of microglia which is likely to contribute to the aberrant phagocytic activities observed in *C9orf72* iPSC-MG mono-cultures.

C9orf72 ALS/FTD postmortem brain tissue analysis validates endosomal-lysosomal pathway dysfunction observed in iPSC-MG

To validate the observed endosomal-lysosomal alterations in *C9orf72* ALS/FTD iPSC-MG, we performed immunohistochemistry on *C9orf72* ALS/FTD patient postmortem brain tissues to examine EEA1 and Lamp1 expression in ionized calcium binding adaptor molecule 1 (Iba-1) positive microglia (Fig. 8; Additional File 7: Table S5). Quantitative analysis of images taken by confocal microscopy revealed increased EEA1 and Lamp1 mean fluorescence intensity per microglia in *C9orf72* ALS/FTD frontal cortex (Fig. 8a-h) and motor cortex (Fig. 8i-p). Interestingly, the observed changes are more significant in the frontal cortex compared to the motor cortex, potentially reflecting the FTD-related cognitive impairments documented for these patient donors

(Additional File 7: Table S5). Importantly, these data are consistent with the iPSC-MG dataset above suggesting a dysfunctional endosomal-lysosomal pathway in *C9orf72* ALS/FTD microglia. In addition, this validation supports the use of this human iPSC-MG *in vitro* model for future studies aimed at elucidating the role of microglia in C9orf72 ALS/FTD disease pathogenesis.

Discussion

An extensive body of evidence has suggested that glia contribute to the neurodegeneration observed in ALS and FTD (9, 10, 110-113). Transcriptional assessments and proteomic approaches across the ALS/FTD spectrum have reported robust glia signatures and glia protein modules, respectively, emphasizing a glia involvement in inflammation and contribution to disease (109, 113-115).

In the present study, we generated microglia from *C9orf72* ALS/FTD patient-derived iPSC to evaluate their cellular and molecular phenotypes. The differentiation protocol was selected based on the transcriptional and functional similarities between the generated human iPSC-MG to adult human microglia as well as for their high purity, yield and distinction from other myeloid cells such as monocytes and dendritic cells (53, 57). The *C9orf72* ALS/FTD iPSC-MG displayed classic microglia characteristics and presented a unique transcriptomic signature profile compared to iPSC-CNs or other glia cell types (71). Applying a list of human microglia-enriched genes from Gosselin and colleagues (52), transcriptional analyses revealed no significant differences between *C9orf72* ALS/FTD and control iPSC-MG under basal, un-stimulated culture conditions. Thus, supporting the notion that the presence of the *C9orf72* HRE does not affect

iPSC microglia differentiation and their baseline transcriptome. As microglia function is strongly influenced by the cellular environment, we examined changes of microglia-enriched genes using existing bulk RNA sequencing data from postmortem *C9orf72* ALS/FTD brain tissues. Surprisingly, no significant changes in the microglia-enriched genes were found either in the frontal, motor or occipital cortex supporting the need for single-cell resolution technologies to better identify changes in gene expression in specific cell populations, similar to what has been reported in Alzheimer's disease brain tissues' analyses (18, 116-120). Cell type-specific analyses from postmortem *C9orf72* ALS/FTD brain tissue will further allow for the identification of subsets of microglia populations and associate their transcriptional signatures with potential neuroprotective or detrimental roles, as well as microglia-specific disease pathways and mechanisms. For example, disease-associated microglia (DAM) represent a microglia subtype which senses and responds to damage through neurodegeneration-associated molecular patterns and is primarily found at sites of neurodegeneration to clear cellular debris and protect neurons from dying (116, 121-127). While the presence of DAM has been suggested in ALS, no detailed investigations on the role of DAM in C9orf72 ALS/FTD has been reported to date.

To our knowledge, this data is the first to indicate that *C9orf72* ALS/FTD iPSC-MG exhibit intrinsic *C9orf72* pathology. Although, transcriptional analysis indicated variability of *C9orf72* mRNA levels across *C9orf72* ALS/FTD iPSC-MG patient lines, no significant differences in *C9orf72* expression were observed by RNA sequencing or qRT-PCR analysis. Our data is consistent with previous studies in iPSC patient-derived neurons and astrocytes (72, 76). However, we observed a significant decrease in C9orf72 protein expression in *C9orf72* iPSC-

MG, which is an interesting finding, as previous reports on *C9orf72* iPSC-astrocytes showed no reduction in C9orf72 protein levels (76). The loss of function of C9orf72 protein has been implicated in alterations of endosomal-lysosomal pathways, hence could certainly contribute to the phagocytic deficits we observed in *C9orf72* iPSC-MG (30, 107, 108, 128-130). Specifically, recent studies performed a detailed analysis on C9orf72 protein localization in control and *C9orf72* ALS/FTD human induced motor neurons (iMNs) and revealed that a large percentage of C9orf72 puncta colocalized with early endosomal marker (EEA1) and Rab5 GTPase, however, not with lysosomal markers such as Lamp1 (108). Additionally, membrane fractionation by centrifugation localized C9orf72 with EEA1 and not with Lamp1. Likewise, when the number of early endosomes, late endosomes and lysosomes where counted in *C9orf72* ALS/FTD iMNs and compared to control iMNs, the loss of lysosomes was the major difference observed between the groups supporting the idea of a potential disruption in the endosomal-lysosomal pathways and consequently, a contribution to neurodegeneration (107, 108). These findings are reinforced by studies reporting enlarged lysosomes in *C9orf72* postmortem patient tissues and previous studies proposing that the function of the C9orf72 protein is linked to the regulation of lysosomes and autophagy (30, 130-133). Our data suggests that similar dysfunctions are present in *C9orf72* microglia as shown in our *in vitro* culture model, but also in *C9orf72* ALS/FTD patient postmortem brain tissues. Further investigations are required to determine if *C9orf72* ALS/FTD iPSC-MG have a decrease in the rate of lysosomal degradation capacity or if a reduction in lysosome numbers due to an impairment of lysosomal biogenesis causes the accumulation of phagocytosed material in these cellular compartments.

We also evaluated the C9orf72 iPSC-MG for the non-canonical translation of DPR proteins, specifically poly-(GP), and detected a significant increase in poly-(GP) levels compared to controls. This is the first documentation of endogenous DPR production in *C9orf72* microglia, suggesting that similar to *C9orf72* iPSC-astrocytes, microglia do undergo repeat-associated non-ATG translation (76). Recent studies have shown neuron-astroglia transmission of *C9orf72* associated DPRs via exosomes in an *in vitro* culture system (134). It is yet to be determined if glia can similarly contribute to transmission of DPRs to neighboring cells.

C9orf72 DPRs have been suggested to contribute to nucleocytoplasmic trafficking defects present in *C9orf72* ALS/FTD neurons (88, 135, 136). One of the consequences of these trafficking defects is the mislocalization of nuclear RNA binding proteins, such as TDP-43. TDP-43 pathology has been shown to be present in glia of *C9orf72* postmortem tissues (85, 87, 137-139). TDP-43 has further been associated with neuroinflammation, microglia neuroprotection and the regulation of microglia phagocytosis (66, 126, 140). In the present study, TDP-43 cytoplasmic accumulations or loss of nuclear TDP-43 was not detected in *C9orf72* ALS/FTD iPSC-MG mono-cultures; similar to what has been observed in *C9orf72* iPSC patient-derived astrocytes (76). Similar to TDP-43, we found no significant difference in the nucleocytoplasmic ratio of the RNA editing protein ADAR2, which has recently been shown by our laboratory to be mislocalized to the cytoplasm of *C9orf72* ALS/FTD iPSC motor neurons, as well as in neurons in *C9orf72* ALS/FTD postmortem tissues and *C9orf72* ALS/FTD mouse model brain tissues (91). The absence of TDP-43 and ADAR2 mislocalization could be due to cellular age of the

differentiated cells, as recent human postmortem tissue studies suggested that TDP-43 mislocalization is a late stage event of ALS pathogenesis (141).

Cerebral spinal fluid and blood cytokine profiles are significantly altered for a large array of cytokines and chemokines in ALS/FTD (142). In addition, recent data support a correlation of specific immune responses of gene-associated ALS subgroups to patient survival (94). As for *C9orf72* ALS/FTD, previous studies in *C9orf72* knockout mice revealed increased IL-6 and IL1β mRNA levels in microglia and an upregulation of inflammatory pathways, suggesting an association between the loss of *C9orf72* and altered microglia function and pro-inflammatory phenotypes (30, 39, 73). Here, *C9orf72* ALS/FTD iPSC-MG mono-cultures exhibit an pro-inflammatory phenotype as supported by significant increases in the inflammatory cytokines IL-1α, IL-6 and TNF-α under basal conditions, and even more so upon LPS stimulation. Further studies are necessary to determine if *C9orf72* ALS/FTD iPSC-MG maintain or exacerbate the inflammatory phenotype or if an anti-inflammatory response is acquired in the presence of *C9orf72* ALS/FTD iPSC-neurons or other glia cell types. IL-1α, TNF and complement component 1q (C1q) are highly expressed and secreted by microglia and are known to be strong inducers of an A1 reactive astrocyte phenotype (71, 143, 144). A1 reactive astrocytes are dysfunctional cells unable to support neuronal synapses that acquire a neurotoxic phenotype driving neuronal death (144, 145).

Conclusions

Overall, we report intrinsic properties of *C9orf72* ALS/FTD iPSC-MG mono-cultures and set the stage for the future use of this model in more mechanistic approaches aimed at understanding the role of microglia in *C9orf72* mediated neurodegeneration. *C9orf72* ALS/FTD iPSC-MG could be used in a 2 or 3-dimensional co-culture system or could be transplanted into *C9orf72* immune deficient mice to further assess microglia contribution to neuronal dysfunction and degeneration in *C9orf72* ALS/FTD. This human cell culture model also provides opportunities for future therapeutic development and drug screening.

Abbreviations

iPSCs: induced pluripotent stem cell; iPSC-MG: induced pluripotent stem cells derived microglia; ALS/FTD: amyotrophic lateral sclerosis/frontotemporal dementia; *C9orf72*: *chromosome 9 open reading frame 72*; HRE: hexanucleotide repeat expansion; G_4C_2: GGGGCC; DPR: dipeptide repeat; TDP-43: TAR-DNA binding protein 43; AD: Alzheimer's disease; CNS: central nervous system; sALS: sporadic ALS; PC: principal component; LPS: lipopolysaccharide; EEA1: early endosome antigen 1; Lamp1: lysosomal associated membrane protein 1; $CD43^+$: cluster of differentiating 43 positive; HPCs: hematopoietic progenitor cells; GFs: growth factors; MBM: microglia basal media; IL-34: interleukin-34; M-CSF: macrophage colony-stimulating factor; TGFβ1: transforming growth factor β1; CD200: cluster of differentiation 200; CX3CL1: fracktaline chemokine C-X3-C motif ligand 1; EBs: embryoid bodies; FB-NIM: Forebrain Neural Induction Media; FB-DM: forebrain neuronal differentiation media; hSN-rodo: human brain synaptoneurosomes fluorescently tagged with pHrodo succinimidyl ester; P2ry12: purinergic surface receptor P2Y12; CX3CR1: C-X3-C Motif Chemokine Receptor 1; TREM2 triggering

receptor expressed on myeloid cells 2; TMEM119: transmembrane protein 119; OPC: oligodendrocyte precursor cells; RAN: repeat associated non-AUG; N/C: nucleocytoplasmic; ADAR2: adenosine deaminase acting on double stranded RNA 2; IL-1: interleukin-1; IL-6: interleukin-6; TNF-α: tumor necrosis factor-α; IL-4: interleukin-4; IL-10: interleukin-10; RabGEF: Rab guanine nucleotide exchange factor; Iba-1: ionized calcium binding adaptor molecule 1; DAM: disease-associated microglia; iMNs: induced motor neurons; C1q: complement component 1q.

Declarations

Acknowledgments

We are grateful for all human tissue samples donated to Target ALS to be made available for our research. We are also thankful for all patients that donated cells for the generation of iPSCs to be used in our studies. We further acknowledge the receipt of iPSC lines through the 'Cedars-Sinai Medical Center's David and Janet Polak Foundation Stem Cell Core Laboratory'. We thank both the Target ALS Consortium and the New York Genome Center for access to their RNA sequencing database. In particular, we would like to thank Drs. Lyle Ostrow and Hemali Phatnani. We would also like to acknowledge Dr. Ramita D. Karra and Dr. Bryan J. Traynor for their technical expertise. We would like to give special thanks to members of the Sattler laboratory for their suggestions and feedback on the manuscript. We would also like to give thanks to Dr. Ileana Soto-Reyes and Dr. Nadine Bakkar for scientific advice and feedback on the manuscript.

Author contributions

IL: Designed experiments, differentiated iPSC-MG, performed and supervised experiments; performed quantitative confocal microscope image analysis; acquired and analyzed data and wrote the manuscript. EA: Performed RNA sequencing analysis for iPSC-MG and human postmortem tissue. JL: Differentiated and maintained iPSC-MG. LMG, BER: Acquired data and performed quantitative microscope image analysis. DL, LB, JS, TAM, TFG: Performed and analyzed experiments. MT, AL, JR: Performed experiments. SM: confocal imaging. CB: Maintained and expanded iPSCs. RP: Manuscript editing. FBG, SA: Provided *C9orf72* iPSC lines. MBJ, AM: Taught first-hand iPSC-MG protocol. TSJ: Provided hSN-rodo. RB, RHB: Provided suggestions and evaluation of our work. KKJ: Designed experiments, provided critical advice and evaluation of our work. RS: Designed experiments, oversaw data analysis and interpretation and participated in manuscript writing, drafting and editing.

Funding

This research was supported by the National Institute on Aging of the National Institutes of Health on the Award Number P30AG019610 (RS). The content is solely the responsibility of the authors and does not necessarily represent the official views of the National Institute of Health. This work was further supported in part by a grant to Cedars-Sinai Medical Center from the Howard Hughes Medical Institute through the James H. Gilliam Fellowships for Advanced Study program. In addition, support was provided through funds by The Robert Packard Center for ALS Research (RS), Barrow Neurological Foundation (RS; RB), The David E. Reese Family Foundation and the George Flaccus Laboratory at TGen for ALS Research (KKJ), Barrow Neurological Foundation postdoctoral fellowship (IL), The Fein Family Foundation (RS; RB), the European Research Council (ERC) under the European Union's Horizon 2020 research and

innovation programme (Grant agreement No. 681181; TSJ), the UK Dementia Research Institute (which receives its funding from DRI Ltd, funded by the UK Medical Research Council, Alzheimer's Society, and Alzheimer's Research UK; TSJ), U.S. Department of Veterans Affairs I01BX003625 (Subaward to RS), NIH/NINDS RO1NS101986 (FBG), NIH/NINDS, RO1NS097545 (RHB), NIH/NINDS T32 NS082174 (AM).

Availability of data and materials

The iPSC-MG and iPSC-CN datasets used and/or analyzed during the current study are available from the corresponding author on reasonable request. All RNA-seq expression data from bulk brain tissue are available through Target ALS/New York Genome Center (http://www.targetals.org/research/resources-for-scientists/resource-genomic-data-sets/).

Ethics approval and consent to participate

Human postmortem tissues for immunohistochemistry experiments were obtained from the Target ALS human postmortem tissue core, which was collected under Target ALS approved patient consent and IRB protocol. Working with de-identified tissues was exempt by the Dignity Health Research Compliance office. For the preparation of human tissue synaptoneurosomes, the use of human tissue for post-mortem studies has been reviewed and approved by the Edinburgh Brain Bank ethics committee and the ACCORD medical research ethics committee, AMREC (approval number 15-HV-016; ACCORD is the Academic and Clinical Central Office for Research and Development, a joint office of the University of Edinburgh and NHS Lothian). The Edinburgh Brain Bank is a Medical Research Council funded facility with research ethics committee (REC) approval (11/ES/0022).

Consent for publication

All authors read and approved the final manuscript.

Competing Interests

The authors declare no competing interests.

References

1. DeJesus-Hernandez M, Mackenzie IR, Boeve BF, Boxer AL, Baker M, Rutherford NJ, et al. Expanded GGGGCC hexanucleotide repeat in noncoding region of C9ORF72 causes chromosome 9p-linked FTD and ALS. Neuron. 2011;72(2):245-56.

2. Renton AE, Majounie E, Waite A, Simon-Sanchez J, Rollinson S, Gibbs JR, et al. A hexanucleotide repeat expansion in C9ORF72 is the cause of chromosome 9p21-linked ALS-FTD. Neuron. 2011;72(2):257-68.

3. Josephs KA, Murray ME, Whitwell JL, Tosakulwong N, Weigand SD, Petrucelli L, et al. Updated TDP-43 in Alzheimer's disease staging scheme. Acta Neuropathol. 2016;131(4):571-85.

4. Neumann M, Sampathu DM, Kwong LK, Truax AC, Micsenyi MC, Chou TT, et al. Ubiquitinated TDP-43 in frontotemporal lobar degeneration and amyotrophic lateral sclerosis. Science. 2006;314(5796):130-3.

5. Ling SC, Polymenidou M, Cleveland DW. Converging mechanisms in ALS and FTD: disrupted RNA and protein homeostasis. Neuron. 2013;79(3):416-38.

6. Lagier-Tourenne C, Polymenidou M, Cleveland DW. TDP-43 and FUS/TLS: emerging roles in RNA processing and neurodegeneration. Hum Mol Genet. 2010;19(R1):R46-64.

7. Nakashima-Yasuda H, Uryu K, Robinson J, Xie SX, Hurtig H, Duda JE, et al. Co-morbidity of TDP-43 proteinopathy in Lewy body related diseases. Acta Neuropathol. 2007;114(3):221-9.

8. Uryu K, Nakashima-Yasuda H, Forman MS, Kwong LK, Clark CM, Grossman M, et al. Concomitant TAR-DNA-binding protein 43 pathology is present in Alzheimer disease and corticobasal degeneration but not in other tauopathies. J Neuropathol Exp Neurol. 2008;67(6):555-64.

9. Ilieva H, Polymenidou M, Cleveland DW. Non-cell autonomous toxicity in neurodegenerative disorders: ALS and beyond. J Cell Biol. 2009;187(6):761-72.

10. Yamanaka K, Chun SJ, Boillee S, Fujimori-Tonou N, Yamashita H, Gutmann DH, et al. Astrocytes as determinants of disease progression in inherited amyotrophic lateral sclerosis. Nat Neurosci. 2008;11(3):251-3.

11. Haidet-Phillips AM, Hester ME, Miranda CJ, Meyer K, Braun L, Frakes A, et al. Astrocytes from familial and sporadic ALS patients are toxic to motor neurons. Nat Biotechnol. 2011;29(9):824-8.

12. Barbeito LH, Pehar M, Cassina P, Vargas MR, Peluffo H, Viera L, et al. A role for astrocytes in motor neuron loss in amyotrophic lateral sclerosis. Brain Res Brain Res Rev. 2004;47(1-3):263-74.

13. Brites D, Vaz AR. Microglia centered pathogenesis in ALS: insights in cell interconnectivity. Front Cell Neurosci. 2014;8:117.

14. Frakes AE, Ferraiuolo L, Haidet-Phillips AM, Schmelzer L, Braun L, Miranda CJ, et al. Microglia induce motor neuron death via the classical NF-kappaB pathway in amyotrophic lateral sclerosis. Neuron. 2014;81(5):1009-23.

15. Yamanaka K, Yamashita H. [ALS and microglia--a player for non-cell-autonomous neuron death]. Brain Nerve. 2007;59(10):1163-70.

16. Kang SH, Li Y, Fukaya M, Lorenzini I, Cleveland DW, Ostrow LW, et al. Degeneration and impaired regeneration of gray matter oligodendrocytes in amyotrophic lateral sclerosis. Nat Neurosci. 2013;16(5):571-9.

17. Prinz M, Jung S, Priller J. Microglia Biology: One Century of Evolving Concepts. Cell. 2019;179(2):292-311.

18. Masuda T, Sankowski R, Staszewski O, Prinz M. Microglia Heterogeneity in the Single-Cell Era. Cell Rep. 2020;30(5):1271-81.

19. Colonna M, Butovsky O. Microglia Function in the Central Nervous System During Health and Neurodegeneration. Annu Rev Immunol. 2017;35:441-68.

20. Bilbo S, Stevens B. Microglia: The Brain's First Responders. Cerebrum. 2017;2017.

21. Hammond TR, Robinton D, Stevens B. Microglia and the Brain: Complementary Partners in Development and Disease. Annu Rev Cell Dev Biol. 2018;34:523-44.

22. Salter MW, Stevens B. Microglia emerge as central players in brain disease. Nat Med. 2017;23(9):1018-27.

23. Stevens B, Schafer DP. Roles of microglia in nervous system development, plasticity, and disease. Dev Neurobiol. 2018;78(6):559-60.

24. Lall D, Baloh RH. Microglia and C9orf72 in neuroinflammation and ALS and frontotemporal dementia. J Clin Invest. 2017;127(9):3250-8.

25. Rostalski H, Leskela S, Huber N, Katisko K, Cajanus A, Solje E, et al. Astrocytes and Microglia as Potential Contributors to the Pathogenesis of C9orf72 Repeat Expansion-Associated FTLD and ALS. Frontiers in neuroscience. 2019;13:486.

26. Trageser KJ, Smith C, Herman FJ, Ono K, Pasinetti GM. Mechanisms of Immune Activation by c9orf72-Expansions in Amyotrophic Lateral Sclerosis and Frontotemporal Dementia. Frontiers in neuroscience. 2019;13:1298.

27. Radford RA, Morsch M, Rayner SL, Cole NJ, Pountney DL, Chung RS. The established and emerging roles of astrocytes and microglia in amyotrophic lateral sclerosis and frontotemporal dementia. Front Cell Neurosci. 2015;9:414.

28. Brettschneider J, Toledo JB, Van Deerlin VM, Elman L, McCluskey L, Lee VM, et al. Microglial activation correlates with disease progression and upper motor neuron clinical symptoms in amyotrophic lateral sclerosis. PLoS One. 2012;7(6):e39216.

29. Brettschneider J, Libon DJ, Toledo JB, Xie SX, McCluskey L, Elman L, et al. Microglial activation and TDP-43 pathology correlate with executive dysfunction in amyotrophic lateral sclerosis. Acta Neuropathol. 2012;123(3):395-407.

30. O'Rourke JG, Bogdanik L, Yanez A, Lall D, Wolf AJ, Muhammad AK, et al. C9orf72 is required for proper macrophage and microglial function in mice. Science. 2016;351(6279):1324-9.

31. Sakae N, Roemer SF, Bieniek KF, Murray ME, Baker MC, Kasanuki K, et al. Microglia in frontotemporal lobar degeneration with progranulin or C9ORF72 mutations. Ann Clin Transl Neurol. 2019;6(9):1782-96.

32. Baker M, Mackenzie IR, Pickering-Brown SM, Gass J, Rademakers R, Lindholm C, et al. Mutations in progranulin cause tau-negative frontotemporal dementia linked to chromosome 17. Nature. 2006;442(7105):916-9.

33. Mizielinska S, Lashley T, Norona FE, Clayton EL, Ridler CE, Fratta P, et al. C9orf72 frontotemporal lobar degeneration is characterised by frequent neuronal sense and antisense RNA foci. Acta Neuropathol. 2013;126(6):845-57.

34. Clement AM, Nguyen MD, Roberts EA, Garcia ML, Boillee S, Rule M, et al. Wild-type nonneuronal cells extend survival of SOD1 mutant motor neurons in ALS mice. Science. 2003;302(5642):113-7.

35. Boillee S, Vande Velde C, Cleveland DW. ALS: a disease of motor neurons and their nonneuronal neighbors. Neuron. 2006;52(1):39-59.

36. Batra R, Lee CW. Mouse Models of C9orf72 Hexanucleotide Repeat Expansion in Amyotrophic Lateral Sclerosis/ Frontotemporal Dementia. Frontiers in cellular neuroscience. 2017;11:196.

37. Jiang J, Zhu Q, Gendron TF, Saberi S, McAlonis-Downes M, Seelman A, et al. Gain of Toxicity from ALS/FTD-Linked Repeat Expansions in C9ORF72 Is Alleviated by Antisense Oligonucleotides Targeting GGGGCC-Containing RNAs. Neuron. 2016;90(3):535-50.

38. Burberry A, Suzuki N, Wang JY, Moccia R, Mordes DA, Stewart MH, et al. Loss-of-function mutations in the C9ORF72 mouse ortholog cause fatal autoimmune disease. Sci Transl Med. 2016;8(347):347ra93.

39. Prudencio M, Belzil VV, Batra R, Ross CA, Gendron TF, Pregent LJ, et al. Distinct brain transcriptome profiles in C9orf72-associated and sporadic ALS. Nat Neurosci. 2015;18(8):1175-82.

40. Lagier-Tourenne C, Baughn M, Rigo F, Sun S, Liu P, Li HR, et al. Targeted degradation of sense and antisense C9orf72 RNA foci as therapy for ALS and frontotemporal degeneration. Proceedings of the National Academy of Sciences of the United States of America. 2013.

41. Zhou Q, Mareljic N, Michaelsen M, Parhizkar S, Heindl S, Nuscher B, et al. Active poly-GA vaccination prevents microglia activation and motor deficits in a C9orf72 mouse model. EMBO Mol Med. 2020;12(2):e10919.

42. Sellgren CM, Sheridan SD, Gracias J, Xuan D, Fu T, Perlis RH. Patient-specific models of microglia-mediated engulfment of synapses and neural progenitors. Mol Psychiatry. 2017;22(2):170-7.

43. Murai N, Mitalipova M, Jaenisch R. Functional analysis of CX3CR1 in human induced pluripotent stem (iPS) cell-derived microglia-like cells. Eur J Neurosci. 2020.

44. Andreone BJ, Przybyla L, Llapashtica C, Rana A, Davis SS, van Lengerich B, et al. Alzheimer's-associated PLCgamma2 is a signaling node required for both TREM2 function and the inflammatory response in human microglia. Nat Neurosci. 2020;23(8):927-38.

45. Butler Iii RR, Kozlova A, Zhang H, Zhang S, Streit M, Sanders AR, et al. The Genetic Relevance of Human Induced Pluripotent Stem Cell-Derived Microglia to Alzheimer's Disease and Major Neuropsychiatric Disorders. Mol Neuropsychiatry. 2020;5(Suppl 1):85-96.

46. Sabogal-Guaqueta AM, Marmolejo-Garza A, de Padua VP, Eggen B, Boddeke E, Dolga AM. Microglia alterations in neurodegenerative diseases and their modeling with human induced pluripotent stem cell and other platforms. Prog Neurobiol. 2020;190:101805.

47. Hasselmann J, Blurton-Jones M. Human iPSC-derived microglia: A growing toolset to study the brain's innate immune cells. Glia. 2020;68(4):721-39.

48. Nugent AA, Lin K, van Lengerich B, Lianoglou S, Przybyla L, Davis SS, et al. TREM2 Regulates Microglial Cholesterol Metabolism upon Chronic Phagocytic Challenge. Neuron. 2020;105(5):837-54 e9.

49. Geirsdottir L, David E, Keren-Shaul H, Weiner A, Bohlen SC, Neuber J, et al. Cross-Species Single-Cell Analysis Reveals Divergence of the Primate Microglia Program. Cell. 2019;179(7):1609-22 e16.

50. Galatro TF, Holtman IR, Lerario AM, Vainchtein ID, Brouwer N, Sola PR, et al. Transcriptomic analysis of purified human cortical microglia reveals age-associated changes. Nat Neurosci. 2017;20(8):1162-71.

51. Smith AM, Dragunow M. The human side of microglia. Trends Neurosci. 2014;37(3):125-35.

52. Gosselin D, Skola D, Coufal NG, Holtman IR, Schlachetzki JCM, Sajti E, et al. An environment-dependent transcriptional network specifies human microglia identity. Science. 2017;356(6344).

53. McQuade A, Coburn M, Tu CH, Hasselmann J, Davtyan H, Blurton-Jones M. Development and validation of a simplified method to generate human microglia from pluripotent stem cells. Mol Neurodegener. 2018;13(1):67.

54. Butovsky O, Jedrychowski MP, Moore CS, Cialic R, Lanser AJ, Gabriely G, et al. Identification of a unique TGF-beta-dependent molecular and functional signature in microglia. Nat Neurosci. 2014;17(1):131-43.

55. Greter M, Lelios I, Pelczar P, Hoeffel G, Price J, Leboeuf M, et al. Stroma-derived interleukin-34 controls the development and maintenance of langerhans cells and the maintenance of microglia. Immunity. 2012;37(6):1050-60.

56. Wang Y, Szretter KJ, Vermi W, Gilfillan S, Rossini C, Cella M, et al. IL-34 is a tissue-restricted ligand of CSF1R required for the development of Langerhans cells and microglia. Nat Immunol. 2012;13(8):753-60.

57. Abud EM, Ramirez RN, Martinez ES, Healy LM, Nguyen CHH, Newman SA, et al. iPSC-Derived Human Microglia-like Cells to Study Neurological Diseases. Neuron. 2017;94(2):278-93 e9.

58. Pandya H, Shen MJ, Ichikawa DM, Sedlock AB, Choi Y, Johnson KR, et al. Differentiation of human and murine induced pluripotent stem cells to microglia-like cells. Nat Neurosci. 2017;20(5):753-9.

59. Abutbul S, Shapiro J, Szaingurten-Solodkin I, Levy N, Carmy Y, Baron R, et al. TGF-beta signaling through SMAD2/3 induces the quiescent microglial phenotype within the CNS environment. Glia. 2012;60(7):1160-71.

60. Chen S, Luo D, Streit WJ, Harrison JK. TGF-beta1 upregulates CX3CR1 expression and inhibits fractalkine-stimulated signaling in rat microglia. J Neuroimmunol. 2002;133(1-2):46-55.

61. Elmore MR, Najafi AR, Koike MA, Dagher NN, Spangenberg EE, Rice RA, et al. Colony-stimulating factor 1 receptor signaling is necessary for microglia viability, unmasking a microglia progenitor cell in the adult brain. Neuron. 2014;82(2):380-97.

62. Barclay AN, Wright GJ, Brooke G, Brown MH. CD200 and membrane protein interactions in the control of myeloid cells. Trends Immunol. 2002;23(6):285-90.

63. Kim KW, Vallon-Eberhard A, Zigmond E, Farache J, Shezen E, Shakhar G, et al. In vivo structure/function and expression analysis of the CX3C chemokine fractalkine. Blood. 2011;118(22):e156-67.

64. Kierdorf K, Prinz M. Factors regulating microglia activation. Front Cell Neurosci. 2013;7:44.

65. Renton AE, Majounie E, Waite A, Simon-Sanchez J, Rollinson S, Gibbs JR, et al. A hexanucleotide repeat expansion in C9ORF72 is the cause of chromosome 9p21-linked ALS-FTD. Neuron. 2011;72(2):257-68.

66. Paolicelli RC, Jawaid A, Henstridge CM, Valeri A, Merlini M, Robinson JL, et al. TDP-43 Depletion in Microglia Promotes Amyloid Clearance but Also Induces Synapse Loss. Neuron. 2017;95(2):297-308 e6.

67. Hesse R, Hurtado ML, Jackson RJ, Eaton SL, Herrmann AG, Colom-Cadena M, et al. Comparative profiling of the synaptic proteome from Alzheimer's disease patients with focus on the APOE genotype. Acta Neuropathol Commun. 2019;7(1):214.

68. Tzioras M, Daniels MJD, King D, Popovic K, Holloway RK, Stevenson AJ, et al. Altered synaptic ingestion by human microglia in Alzheimer's disease. BioRxiv. 2019.

69. Balez R, Steiner N, Engel M, Munoz SS, Lum JS, Wu Y, et al. Neuroprotective effects of apigenin against inflammation, neuronal excitability and apoptosis in an induced pluripotent stem cell model of Alzheimer's disease. Scientific reports. 2016;6:31450.

70. Muffat J, Li Y, Yuan B, Mitalipova M, Omer A, Corcoran S, et al. Efficient derivation of microglia-like cells from human pluripotent stem cells. Nat Med. 2016;22(11):1358-67.

71. Zhang Y, Chen K, Sloan SA, Bennett ML, Scholze AR, O'Keeffe S, et al. An RNA-sequencing transcriptome and splicing database of glia, neurons, and vascular cells of the cerebral cortex. J Neurosci. 2014;34(36):11929-47.

72. Sareen D, O'Rourke JG, Meera P, Muhammad AK, Grant S, Simpkinson M, et al. Targeting RNA foci in iPSC-derived motor neurons from ALS patients with a C9ORF72 repeat expansion. Sci Transl Med. 2013;5(208):208ra149.

73. Lagier-Tourenne C, Baughn M, Rigo F, Sun S, Liu P, Li HR, et al. Targeted degradation of sense and antisense C9orf72 RNA foci as therapy for ALS and frontotemporal degeneration. Proc Natl Acad Sci U S A. 2013;110(47):E4530-9.

74. Mackenzie IR, Arzberger T, Kremmer E, Troost D, Lorenzl S, Mori K, et al. Dipeptide repeat protein pathology in C9ORF72 mutation cases: clinico-pathological correlations. Acta Neuropathol. 2013;126(6):859-79.

75. Ash PE, Bieniek KF, Gendron TF, Caulfield T, Lin WL, Dejesus-Hernandez M, et al. Unconventional translation of C9ORF72 GGGGCC expansion generates insoluble polypeptides specific to c9FTD/ALS. Neuron. 2013;77(4):639-46.

76. Zhao C, Devlin AC, Chouhan AK, Selvaraj BT, Stavrou M, Burr K, et al. Mutant C9orf72 human iPSC-derived astrocytes cause non-cell autonomous motor neuron pathophysiology. Glia. 2020;68(5):1046-64.

77. Donnelly CJ, Zhang PW, Pham JT, Haeusler AR, Mistry NA, Vidensky S, et al. RNA toxicity from the ALS/FTD C9ORF72 expansion is mitigated by antisense intervention. Neuron. 2013;80(2):415-28.

78. Zhang YJ, Gendron TF, Grima JC, Sasaguri H, Jansen-West K, Xu YF, et al. C9ORF72 poly(GA) aggregates sequester and impair HR23 and nucleocytoplasmic transport proteins. Nat Neurosci. 2016;19(5):668-77.

79. Freibaum BD, Taylor JP. The Role of Dipeptide Repeats in C9ORF72-Related ALS-FTD. Front Mol Neurosci. 2017;10:35.

80. Gendron TF, Chew J, Stankowski JN, Hayes LR, Zhang YJ, Prudencio M, et al. Poly(GP) proteins are a useful pharmacodynamic marker for C9ORF72-associated amyotrophic lateral sclerosis. Sci Transl Med. 2017;9(383).

81. Jiang J, Cleveland DW. Bidirectional Transcriptional Inhibition as Therapy for ALS/FTD Caused by Repeat Expansion in C9orf72. Neuron. 2016;92(6):1160-3.

82. O'Rourke JG, Bogdanik L, Muhammad A, Gendron TF, Kim KJ, Austin A, et al. C9orf72 BAC Transgenic Mice Display Typical Pathologic Features of ALS/FTD. Neuron. 2015;88(5):892-901.

83. Zu T, Liu Y, Banez-Coronel M, Reid T, Pletnikova O, Lewis J, et al. RAN proteins and RNA foci from antisense transcripts in C9ORF72 ALS and frontotemporal dementia. Proceedings of the National Academy of Sciences of the United States of America. 2013.

84. Andrade NS, Ramic M, Esanov R, Liu W, Rybin MJ, Gaidosh G, et al. Dipeptide repeat proteins inhibit homology-directed DNA double strand break repair in C9ORF72 ALS/FTD. Mol Neurodegener. 2020;15(1):13.

85. Cooper-Knock J, Hewitt C, Highley JR, Brockington A, Milano A, Man S, et al. Clinico-pathological features in amyotrophic lateral sclerosis with expansions in C9ORF72. Brain. 2012;135(Pt 3):751-64.

86. Al-Sarraj S, King A, Troakes C, Smith B, Maekawa S, Bodi I, et al. p62 positive, TDP-43 negative, neuronal cytoplasmic and intranuclear inclusions in the cerebellum and hippocampus define the pathology of C9orf72-linked FTLD and MND/ALS. Acta Neuropathol. 2011;122(6):691-702.

87. Schipper LJ, Raaphorst J, Aronica E, Baas F, de Haan R, de Visser M, et al. Prevalence of brain and spinal cord inclusions, including dipeptide repeat proteins, in patients with the C9ORF72 hexanucleotide repeat expansion: a systematic neuropathological review. Neuropathol Appl Neurobiol. 2016;42(6):547-60.

88. Moore S, Rabichow BE, Sattler R. The Hitchhiker's Guide to Nucleocytoplasmic Trafficking in Neurodegeneration. Neurochem Res. 2020;45(6):1306-27.

89. Zhang K, Donnelly CJ, Haeusler AR, Grima JC, Machamer JB, Steinwald P, et al. The C9orf72 repeat expansion disrupts nucleocytoplasmic transport. Nature. 2015;525(7567):56-61.

90. Chou CC, Zhang Y, Umoh ME, Vaughan SW, Lorenzini I, Liu F, et al. TDP-43 pathology disrupts nuclear pore complexes and nucleocytoplasmic transport in ALS/FTD. Nat Neurosci. 2018;21(2):228-39.

91. Moore S, Alsop E, Lorenzini I, Starr A, Rabichow BE, Mendez E, et al. ADAR2 mislocalization and widespread RNA editing aberrations in C9orf72-mediated ALS/FTD. Acta Neuropathol. 2019;138(1):49-65.

92. Smith JA, Das A, Ray SK, Banik NL. Role of pro-inflammatory cytokines released from microglia in neurodegenerative diseases. Brain Res Bull. 2012;87(1):10-20.

93. Moreno-Martinez L, Calvo AC, Munoz MJ, Osta R. Are Circulating Cytokines Reliable Biomarkers for Amyotrophic Lateral Sclerosis? Int J Mol Sci. 2019;20(11).

94. Olesen MN, Wuolikainen A, Nilsson AC, Wirenfeldt M, Forsberg K, Madsen JS, et al. Inflammatory profiles relate to survival in subtypes of amyotrophic lateral sclerosis. Neurol Neuroimmunol Neuroinflamm. 2020;7(3).

95. McCauley ME, Baloh RH. Inflammation in ALS/FTD pathogenesis. Acta Neuropathol. 2019;137(5):715-30.

96. Beers DR, Appel SH. Immune dysregulation in amyotrophic lateral sclerosis: mechanisms and emerging therapies. Lancet Neurol. 2019;18(2):211-20.

97. Paresce DM, Ghosh RN, Maxfield FR. Microglial cells internalize aggregates of the Alzheimer's disease amyloid beta-protein via a scavenger receptor. Neuron. 1996;17(3):553-65.

98. Stevens B, Allen NJ, Vazquez LE, Howell GR, Christopherson KS, Nouri N, et al. The classical complement cascade mediates CNS synapse elimination. Cell. 2007;131(6):1164-78.

99. Bialas AR, Stevens B. TGF-beta signaling regulates neuronal C1q expression and developmental synaptic refinement. Nature neuroscience. 2013;16(12):1773-82.

100. Tremblay ME, Stevens B, Sierra A, Wake H, Bessis A, Nimmerjahn A. The role of microglia in the healthy brain. J Neurosci. 2011;31(45):16064-9.

101. Hong S, Beja-Glasser VF, Nfonoyim BM, Frouin A, Li S, Ramakrishnan S, et al. Complement and microglia mediate early synapse loss in Alzheimer mouse models. Science. 2016;352(6286):712-6.

102. Lui H, Zhang J, Makinson SR, Cahill MK, Kelley KW, Huang HY, et al. Progranulin Deficiency Promotes Circuit-Specific Synaptic Pruning by Microglia via Complement Activation. Cell. 2016;165(4):921-35.

103. Colom-Cadena M, Spires-Jones T, Zetterberg H, Blennow K, Caggiano A, DeKosky ST, et al. The clinical promise of biomarkers of synapse damage or loss in Alzheimer's disease. Alzheimers Res Ther. 2020;12(1):21.

104. Henstridge CM, Pickett E, Spires-Jones TL. Synaptic pathology: a shared mechanism in neurological disease. Ageing Res Rev. 2016.

105. Levine TP, Daniels RD, Gatta AT, Wong LH, Hayes MJ. The product of C9orf72, a gene strongly implicated in neurodegeneration, is structurally related to DENN Rab-GEFs. Bioinformatics. 2013;29(4):499-503.

106. Aoki Y, Manzano R, Lee Y, Dafinca R, Aoki M, Douglas AGL, et al. C9orf72 and RAB7L1 regulate vesicle trafficking in amyotrophic lateral sclerosis and frontotemporal dementia. Brain. 2017;140(4):887-97.

107. Farg MA, Sundaramoorthy V, Sultana JM, Yang S, Atkinson RA, Levina V, et al. C9ORF72, implicated in amytrophic lateral sclerosis and frontotemporal dementia, regulates endosomal trafficking. Hum Mol Genet. 2014;23(13):3579-95.

108. Shi Y, Lin S, Staats KA, Li Y, Chang WH, Hung ST, et al. Haploinsufficiency leads to neurodegeneration in C9ORF72 ALS/FTD human induced motor neurons. Nat Med. 2018;24(3):313-25.

109. Umoh ME, Dammer EB, Dai J, Duong DM, Lah JJ, Levey AI, et al. A proteomic network approach across the ALS-FTD disease spectrum resolves clinical phenotypes and genetic vulnerability in human brain. EMBO Mol Med. 2018;10(1):48-62.

110. Ban J, Samano C, Mladinic M, Munitic I. Glia in amyotrophic lateral sclerosis and spinal cord injury: common therapeutic targets. Croat Med J. 2019;60(2):109-20.

111. Filipi T, Hermanova Z, Tureckova J, Vanatko O, Anderova AM. Glial Cells-The Strategic Targets in Amyotrophic Lateral Sclerosis Treatment. J Clin Med. 2020;9(1).

112. Valori CF, Guidotti G, Brambilla L, Rossi D. Astrocytes in Motor Neuron Diseases. Adv Exp Med Biol. 2019;1175:227-72.

113. Dols-Icardo O, Montal V, Sirisi S, Lopez-Pernas G, Cervera-Carles L, Querol-Vilaseca M, et al. Motor cortex transcriptome reveals microglial key events in amyotrophic lateral sclerosis. Neurol Neuroimmunol Neuroinflamm. 2020;7(5).

114. Tam OH, Rozhkov NV, Shaw R, Kim D, Hubbard I, Fennessey S, et al. Postmortem Cortex Samples Identify Distinct Molecular Subtypes of ALS: Retrotransposon Activation, Oxidative Stress, and Activated Glia. Cell Rep. 2019;29(5):1164-77 e5.

115. D'Erchia AM, Gallo A, Manzari C, Raho S, Horner DS, Chiara M, et al. Massive transcriptome sequencing of human spinal cord tissues provides new insights into motor neuron degeneration in ALS. Sci Rep. 2017;7(1):10046.

116. Keren-Shaul H, Spinrad A, Weiner A, Matcovitch-Natan O, Dvir-Szternfeld R, Ulland TK, et al. A Unique Microglia Type Associated with Restricting Development of Alzheimer's Disease. Cell. 2017;169(7):1276-90 e17.

117. Mrdjen D, Pavlovic A, Hartmann FJ, Schreiner B, Utz SG, Leung BP, et al. High-Dimensional Single-Cell Mapping of Central Nervous System Immune Cells Reveals Distinct Myeloid Subsets in Health, Aging, and Disease. Immunity. 2018;48(2):380-95 e6.

118. Bottcher C, Schlickeiser S, Sneeboer MAM, Kunkel D, Knop A, Paza E, et al. Human microglia regional heterogeneity and phenotypes determined by multiplexed single-cell mass cytometry. Nat Neurosci. 2019;22(1):78-90.

119. Masuda T, Sankowski R, Staszewski O, Bottcher C, Amann L, Sagar, et al. Spatial and temporal heterogeneity of mouse and human microglia at single-cell resolution. Nature. 2019;566(7744):388-92.

120. Sankowski R, Bottcher C, Masuda T, Geirsdottir L, Sagar, Sindram E, et al. Mapping microglia states in the human brain through the integration of high-dimensional techniques. Nat Neurosci. 2019;22(12):2098-110.

121. Ajami B, Samusik N, Wieghofer P, Ho PP, Crotti A, Bjornson Z, et al. Single-cell mass cytometry reveals distinct populations of brain myeloid cells in mouse neuroinflammation and neurodegeneration models. Nat Neurosci. 2018;21(4):541-51.

122. Friedman BA, Srinivasan K, Ayalon G, Meilandt WJ, Lin H, Huntley MA, et al. Diverse Brain Myeloid Expression Profiles Reveal Distinct Microglial Activation States and Aspects of Alzheimer's Disease Not Evident in Mouse Models. Cell Rep. 2018;22(3):832-47.

123. Holtman IR, Raj DD, Miller JA, Schaafsma W, Yin Z, Brouwer N, et al. Induction of a common microglia gene expression signature by aging and neurodegenerative conditions: a co-expression meta-analysis. Acta Neuropathol Commun. 2015;3:31.

124. Chiu IM, Morimoto ET, Goodarzi H, Liao JT, O'Keeffe S, Phatnani HP, et al. A neurodegeneration-specific gene-expression signature of acutely isolated microglia from an amyotrophic lateral sclerosis mouse model. Cell Rep. 2013;4(2):385-401.

125. Krasemann S, Madore C, Cialic R, Baufeld C, Calcagno N, El Fatimy R, et al. The TREM2-APOE Pathway Drives the Transcriptional Phenotype of Dysfunctional Microglia in Neurodegenerative Diseases. Immunity. 2017;47(3):566-81 e9.

126. Spiller KJ, Restrepo CR, Khan T, Dominique MA, Fang TC, Canter RG, et al. Microglia-mediated recovery from ALS-relevant motor neuron degeneration in a mouse model of TDP-43 proteinopathy. Nat Neurosci. 2018;21(3):329-40.

127. Deczkowska A, Keren-Shaul H, Weiner A, Colonna M, Schwartz M, Amit I. Disease-Associated Microglia: A Universal Immune Sensor of Neurodegeneration. Cell. 2018;173(5):1073-81.

128. Amick J, Roczniak-Ferguson A, Ferguson SM. C9orf72 binds SMCR8, localizes to lysosomes, and regulates mTORC1 signaling. Mol Biol Cell. 2016;27(20):3040-51.

129. Amick J, Tharkeshwar AK, Talaia G, Ferguson SM. PQLC2 recruits the C9orf72 complex to lysosomes in response to cationic amino acid starvation. J Cell Biol. 2020;219(1).

130. Sullivan PM, Zhou X, Robins AM, Paushter DH, Kim D, Smolka MB, et al. The ALS/FTLD associated protein C9orf72 associates with SMCR8 and WDR41 to regulate the autophagy-lysosome pathway. Acta Neuropathol Commun. 2016;4(1):51.

131. Shao Q, Yang M, Liang C, Ma L, Zhang W, Jiang Z, et al. C9orf72 and smcr8 mutant mice reveal MTORC1 activation due to impaired lysosomal degradation and exocytosis. Autophagy. 2019:1-16.

132. Amick J, Ferguson SM. C9orf72: At the intersection of lysosome cell biology and neurodegenerative disease. Traffic. 2017;18(5):267-76.

133. Wang M, Wang H, Tao Z, Xia Q, Hao Z, Prehn JHM, et al. C9orf72 associates with inactive Rag GTPases and regulates mTORC1-mediated autophagosomal and lysosomal biogenesis. Aging cell. 2020:e13126.

134. Westergard T, Jensen BK, Wen X, Cai J, Kropf E, Iacovitti L, et al. Cell-to-Cell Transmission of Dipeptide Repeat Proteins Linked to C9orf72-ALS/FTD. Cell Rep. 2016;17(3):645-52.

135. Jovicic A, Mertens J, Boeynaems S, Bogaert E, Chai N, Yamada SB, et al. Modifiers of C9orf72 dipeptide repeat toxicity connect nucleocytoplasmic transport defects to FTD/ALS. Nat Neurosci. 2015;18(9):1226-9.

136. Boeynaems S, Bogaert E, Michiels E, Gijselinck I, Sieben A, Jovicic A, et al. Drosophila screen connects nuclear transport genes to DPR pathology in c9ALS/FTD. Scientific reports. 2016;6:20877.

137. Brettschneider J, Arai K, Del Tredici K, Toledo JB, Robinson JL, Lee EB, et al. TDP-43 pathology and neuronal loss in amyotrophic lateral sclerosis spinal cord. Acta Neuropathol. 2014;128(3):423-37.

138. Fatima M, Tan R, Halliday GM, Kril JJ. Spread of pathology in amyotrophic lateral sclerosis: assessment of phosphorylated TDP-43 along axonal pathways. Acta Neuropathol Commun. 2015;3:47.

139. Yamanaka K, Komine O. The multi-dimensional roles of astrocytes in ALS. Neurosci Res. 2018;126:31-8.

140. Swarup V, Phaneuf D, Dupre N, Petri S, Strong M, Kriz J, et al. Deregulation of TDP-43 in amyotrophic lateral sclerosis triggers nuclear factor kappaB-mediated pathogenic pathways. J Exp Med. 2011;208(12):2429-47.

141. Vatsavayai SC, Yoon SJ, Gardner RC, Gendron TF, Vargas JN, Trujillo A, et al. Timing and significance of pathological features in C9orf72 expansion-associated frontotemporal dementia. Brain. 2016;139(Pt 12):3202-16.

142. Lu CH, Allen K, Oei F, Leoni E, Kuhle J, Tree T, et al. Systemic inflammatory response and neuromuscular involvement in amyotrophic lateral sclerosis. Neurol Neuroimmunol Neuroinflamm. 2016;3(4):e244.

143. Bennett ML, Bennett FC, Liddelow SA, Ajami B, Zamanian JL, Fernhoff NB, et al. New tools for studying microglia in the mouse and human CNS. Proc Natl Acad Sci U S A. 2016;113(12):E1738-46.

144. Liddelow SA, Guttenplan KA, Clarke LE, Bennett FC, Bohlen CJ, Schirmer L, et al. Neurotoxic reactive astrocytes are induced by activated microglia. Nature. 2017;541(7638):481-7.

145. Liddelow SA, Marsh SE, Stevens B. Microglia and Astrocytes in Disease: Dynamic Duo or Partners in Crime? Trends Immunol. 2020.

Figure Legends

Fig. 1 Healthy control and *C9orf72* ALS/FTD patient iPSC lines differentiate into mature microglia**.** (**a**) Schematic illustration of iPSC-MG differentiation protocol (adapted from (53, 57)). (**b**) Phase contrast images of mature iPSC-MG differentiated from healthy control and *C9orf72* ALS/FTD iPSCs (DIV 40). The representative images show typical ramified microglia morphology in both experimental groups. Scale bar, 120µm. (**c**) Representative immunofluorescence of DIV 40 control (n=5) and *C9orf72* ALS/FTD iPSC-MG (n=7) stained for myeloid transcription factor PU.1 and microglia specific markers such as purinergic surface

receptor P2ry12, C-X3-C Motif Chemokine Receptor 1 (Cx3cr1), triggering receptor expressed on myeloid cells 2 (TREM2) and the transmembrane protein 119 (TMEM119). See Additional file: Figure S1a-b. Scale bar, 15µm. (**d**) Heatmap of the complete iPSC-MG (control, n=4 cell lines with 1-2 differentiations each and *C9orf72* ALS/FTD, n=7 cell lines with 1-2 differentiations each) and iPSC-CN (n=12 cell lines with 1-3 differentiations each) transcriptome demonstrating distinct gene expression profiles between the two cell populations. All iPSC-MG and iPSC-CN samples were normalized together by DESeq2 and Z-score scaled. (**e**) Principal component analysis of the RNA-seq expression data revealed a highly similar gene expression profile within both iPSC-MG and iPSC-CNs (green cluster) (PC2, 1.66% variance) and confirmed these populations as distinct from each other (blue cluster) (PC1, 94.87% variance). (**f**) Normalized counts for genes associated with microglia, astrocytes, oligo-precursor cells (OPC), oligodendrocytes, neurons, endothelial cells and pericytes within the iPSC-MG population (Control n=4 lines; *C9orf72* ALS/FTD n=7 lines). Gene list from (71). Bar graphs are presented as mean ± SD. Heatmaps were generated using z-scores calculated from DESeq2 normalized gene counts. Principal component analysis was done using DESeq2 normalized gene counts with the PCAExplorer package (v. 2.14.1) in R. Bar graphs show normalized gene counts per iPSC-MG group generated from the RNA sequencing presented as Mean ± SD.

Fig. 2 Minor transcriptional changes in *C9orf72* ALS/FTD iPSC-MG and in postmortem tissues of *C9orf72* ALS/FTD patients. Illumina RNA sequencing analysis was assessed on mature (DIV 40) iPSC-MG for overall gene expression changes and for the presence of dysregulated microglia-enriched genes, as defined recently (52). Additionally, human motor cortex and frontal

cortex RNA sequencing data sets obtained through Target ALS were used to identify transcriptional changes. (**a**) Volcano plot showing differentially expressed transcripts between healthy control (n=4) and *C9orf72* ALS/FTD (n=7) from the full iPSC-MG transcriptome (unadjusted p value <0.005; $\log_2$ fold change (FC) ± 1). (**b**) Volcano plot of differentially expressed microglia-enriched transcripts indicates that there are no significant expression changes of these particular genes in mono-cultures of *C9orf72* ALS/FTD iPSC-MG (n=7) compared to healthy control (n=4) (unadjusted p value <0.005; $\log_2$ fold change (FC) ± 1). (**c-d**) Existing RNA sequencing data from postmortem autopsy brain tissues (frontal cortex, motor cortex of *C9orf72* ALS/FTD patients and controls) were also analyzed for differentially expressed 881 microglia-enriched transcripts. Few differentially expressed microglia transcripts in *C9orf72* ALS/FTD were observed compared to controls (See Additional File 2: Figure S2b-d). Number of brain tissue samples included in the analyses: frontal cortex (control n=16; *C9orf72* ALS/FTD n=8), motor cortex (control n=15; *C9orf72* ALS/FTD n=12) and occipital cortex (control n=4; *C9orf72* ALS/FTD n=5) (unadjusted p value <0.005; $\log_2$ fold change (FC) ± 1). Volcano plots were generated from DESeq2 output using EnhancedVolcano. All statistical analysis was done in R (version 3.6.2) using raw counts matrices from featureCounts as input. Low expression genes were filtered such that genes with mean read counts < 10 were removed from the analysis. Differential expression analysis was done using DESeq2 (version 1.26.0) using disease status as the model. Tissue data from Target ALS was downloaded from the New York Genome Center as raw fastq files and pushed through an identical analysis pipeline as data generated for the iPSC-MGs.

Fig. 3 *C9orf72* ALS/FTD iPSC-MG exhibit reduced C9orf72 protein expression and produce poly-(GP) DPR protein. RNA sequencing, qRT-PCR, Western Blots and C9orf72 protein immunolabeling were performed to determine changes in *C9orf72* gene and protein expression levels. In addition, an ELISA assay was used to measure poly-(GP) abundance in iPSC-MG. (**a**) Dot plot showing *C9orf72* level of expression as log2 (counts +1) in control and *C9orf72* ALS/FTD iPSC-MG (normalized mean count in control, 855.37, n=4 lines; *C9orf72*, 772.08, n=7 lines; p-value = 0.66, Student's t- test). No differences were observed. (**b**) Relative human *C9orf72* mRNA expression in control and *C9orf72* ALS/FTD iPSC-MG (normalized to beta-2-microglobulin (B2M) in control, 0.99, n=3 lines, n=1-4 differentiation per line; *C9orf72*, 1, n=6 lines, n=1-3 differentiation per line; p-value = 0.8; Student's t-test). No differences between groups were detected. (**c**) Western blot analysis shows a reduction in human C9orf72 protein expression in *C9orf72* ALS/FTD iPSC-MG. 50kDa C9orf72 protein band highlighted with a green arrow. (control, n=3 lines, n=1-2 differentiation per line; *C9orf72*, n=5 lines, n=1-2 differentiation per line). (**d**) Quantification of *C9orf72* western blot analysis revealed significant reduction in C9orf72 protein levels (normalized to tubulin in control, 99.52, n=3 lines, n=1-2 differentiation per line; *C9orf72*, 60.41, n=5 lines, n=1-2 differentiation per line; p-value = 0.006; Student's t-test). (**e**) Immunofluorescence for C9orf72 protein in iPSC-MG confirms reduced C9orf72 protein expression in *C9orf72* microglia. (**f**) A significant increase in intracellular levels of poly-(GP) was detected in *C9orf72* ALS/FTD iPSC-MG using an ELISA assay (relative abundance of poly-(GP) in control, 5.46, n = 3 lines; *C9orf72,* 46.18, n = 7 lines, p=0.0167, two tailed Mann Whitney test). Data is presented as Median ± SEM for *C9orf72* level expression. Student's t-test was performed

for qRT-PCR and WB analysis. Data is presented as Mean ± SEM . Two tailed Mann Whitney test was performed for the poly-(GP) ELISA assay. ** *p*-value < 0.01, * *p*-value < 0.05.

Fig. 4 *C9orf72* ALS/FTD iPSC-MG respond with increased cytokine release upon LPS stimulation. IPSC-MGs were treated with LPS (100ng/ml) for 6hr. The conditioned media was collected and analyzed for a cytokine/chemokine profile using the V-plex human cytokines kit (Mesoscale). Under basal conditions, *C9orf72* ALS/FTD iPSC-MG monocultures showed a significant increase in IL-1α, IL-6 and TNF-α inflammatory cytokines compared to controls. Upon LPS stimulation, *C9orf72* ALS/FTD iPSC-MG released higher levels of IL-1α, IL-1β and IL-6 cytokines than under basal conditions and compared to control iPSC-MG. Data presented as the concentration of secreted proteins (pg/ml), Mean ± SEM, n=2 control lines; n=2 *C9orf72* lines; * $p \leq 0.05$; ** $p \leq 0.01$; **** $p \leq 0.0001$; multiple t-test corrected for multiple comparison using Holm-Sidak method.

Fig. 5 *C9orf72* ALS/FTD iPSC-MGs phagocytose Aβ (1-40). IPSC-MG engulf and degrade Aβ (1-40) TAMRA. After a 5 minute treatment with 1μM Aβ (1-40) TAMRA, iPSC-MG were washed, fixed and immunostained at 5 min, 30 min and 1 h. (**a**-**b**; **g**-**h**) Control and *C9orf72* ALS/FTD iPSC-MG stained for TREM2 (green) and highlighting Aβ (1-40) TAMRA (red) inside the cells at the 30 minutes time point. White arrows point at phagocytic cells containing Aβ (1-40) TAMRA (red). Scale bar, 20µm. (**c**, **i**) Aβ (1-40) TAMRA (red) internalized by controls and *C9orf72* ALS/FTD iPSC-MG. *C9orf72* ALS/FTD iPSC-MG have a significant increase in area covered by Aβ (1-40) compared to control group. Scale bar, 20µm. (**d**-**e**; **j**-**k**) 3D view (scale bar, 15µm) and

extended view (**f**, **l**) showing phagocytic activity in both iPSC-MG groups. Scale bar, 20µm. (**m**) No changes were observed at 5 minutes (percentage of cell surface area covered by Aβ (1-40)-TAMRA in control, 18.69, n=2 lines; *C9orf72*, 19.07, n=5 lines; n= 1-2 differentiations per line p = 0.72 using Student's t-test). A significant reduction in Aβ (1-40) TAMRA clearance was seen at 30 minutes (percentage of cell surface area covered by Aβ (1-40)-TAMRA in control, 11.8, n=2 lines; *C9orf72*, 13.20, n=5 lines; n= 1-2 differentiations per line; n = 55-275 cells/ group; *p = 0.037 using Student's t-test) and 1 h (percentage of cell surface area covered by Aβ (1-40)-TAMRA in control, 4.3, n=2 lines; *C9orf72*, 5.2, n=5 lines; n= 1-2 differentiations per line; n = 55-275 cells/ group; *p = 0.024 using Student's t-test) in *C9orf72*-iPSC-MGs compared to controls. (**n**) No differences in cell surface area were observed (area in control, 2020 μm^2, n=2 lines; *C9orf72*, 2084 μm^2, n=5 lines; n= 1-2 differentiations per line; n = 55-275 cells/ group; p = 0.3 using Student's t-test). Data presented as Mean ± SEM, $*p < 0.05$; Student's t-test.

Fig. 6 Phagocytic uptake of human brain synaptoneurosomes by iPSC-MGs. (**a**) Illustration of iPSC-MGs treated with human brain synaptoneurosomes. IPSC-MGs (Day 40) are labeled with nuclear maker Hoechst (cyan) followed by hSN-rodo treatment (orange) ± 10µM Cytochalasin D (actin polymerization inhibitor). (**b**-**e**) Control and (**f**-**i**) *C9orf72* ALS/FTD iPSC-MG images taken at 0 h time point using confocal microscopy with differential interference contrast . No evident phagocytosis of hSN-rodo is seen at this time point (**c**, **e**; **g**, **i**). Scale bars = 50µm. (**j**-**k**) Control and (**n**-**o**) *C9orf72* ALS/FTD iPSC-MG at 2 h show an increase in hSN-rodo fluorescent signal inside iPSC-MG indicative of phagocytosis and uptake into intracellular acidic compartments. Scale bar = 40μm. (**l**-**m**; **p**-**q**) Higher magnification representative images

highlighting the increase in hSN-rodo signal in individual iPSC-MG at 2 h. Scale bar = 10μm. (**r**) Percentage of iPSC-MG engulfing hSN-rodo during the 6 h time course of live imaging. At 2 h, control and *C9orf72* iPSC-MG showed 69% and 71% phagocytic activity, respectively. No differences in synaptoneurosome uptake was observed. 10uM cytochalasin D was used as a negative control to inhibit phagocytic activity in iPSC-MGs (control, n=1 line; *C9orf72,* n=2 lines; n = 70-115 average cells/ image/ group; n =18 images/group/ time point for hSN-rodo; for cytochalasin D, n = 70-115 average cells/ image/ group; n =6 images/group/ time point). (**s**) Quantification of hSN-rodo mean intensity per cell at 2 h revealed increased uptake in *C9orf72* ALS/FTD iPSC-MG (control, n=1 line, 1594; *C9orf72,* n=2 lines, 1820; n = 6-10 cells/ image/ group, n = 18 images for 2 h time point; *p value =0.02, Student's t-test; n = 7-10 cells/ image/ group; for cytochalasin D, control, n=1 line, 845; *C9orf72,* n=2 lines, 1106, n =6 images/group/ time point; ***p value =0.0007, Student's t-test). Data presented as Mean intensity ± SEM, ****p* value ≤ 0.001, **p*-value < 0.05.

Fig. 7 Alterations in early endosomal and lysosomal protein expression in *C9orf72* ALS/FTD iPSC-MGs. Immunocytochemistry, 3 dimensional image analysis and RNA sequencing were used to detect changes in endosomal and lysosomal protein and mRNA levels in *C9orf72* iPSC-MG. (**a**-**b**) Outlined 3D cell surface volume of each control and *C9orf72* ALS/FTD iPSC-MGs stained for EEA1 and DAPI. Scale bar, 20µm. (**c**) A significant increase in mean fluorescence intensity of EEA1 was observed in *C9orf72* ALS/FTD iPSC-MGs compared to controls. (control n=2 lines, 3775 AU, n=90-150 cells per line; *C9orf72*, 4308 AU, n=2 lines, n=100-150 cells per line; ****p value =0.0001 using Student's t-test). (**d**-**e**) Control and *C9orf72* ALS/FTD iPSC-MGs

stained for Lamp1 and DAPI. Scale bar, 20µm. (**f**) A reduction in Lamp1 in *C9orf72* ALS/FTD iPSC-MGs was observed (mean fluorescence intensity in control n=2 lines, 1328 AU, n=90-150 cells per line; *C9orf72*, n=2 lines, 715.3 AU, n=100-150 cells per line; ****p value =0.0001 using Student's t-test). (**g**-**h**) Merge view of control and *C9orf72* ALS/FTD iPSC-MGs stained for EEA1, Lamp1 and DAPI. Scale bar, 20µm. (**i**) No changes in iPSC-MGs cell surface volume was observed (control n=2 lines, 2050 μm^3, n=90-150 cells per line; *C9orf72*, n=2 lines, 2132 μm^3, n=100-150 cells per line; p value =0.24 using Student's t-test). (**j**) No significant changes in normalized gene counts for endosomal-lysosomal genes in control and *C9orf72* ALS/FTD iPSC-MGs obtained from RNA seq analyses of unstimulated iPSC-MGs mono-cultures. Data is presented as the Mean ± SEM. Student's t-test, ****$p < 0.0001$.

Fig. 8 Aberrant EEA1 and Lamp1 expression in microglia in *C9orf72* ALS/FTD patient postmortem tissues. *C9orf72* ALS/FTD patient postmortem frontal and motor cortex were immunostained for EEA1 and Lamp1 (Additional File 7: Table S5). (**a**-**b**; **i**-**j**) Control and *C9orf72* ALS/FTD microglia stained for Iba-1, EEA1 and DAPI in areas of the frontal and motor cortex of *C9orf72* ALS/FTD patients. Scale bar, 5µm. (**c**, **k**) Extended view image of *C9orf72* ALS/FTD microglia show EEA1 accumulations inside microglia in both frontal and motor cortex. Scale bar, 5µm. (**d**, **l**) A significant increase in EEA1 mean intensity was observed in microglia of the frontal cortex (mean fluorescence intensity in control, 745200 AU; *C9orf72*, 3160465 AU; n=2 cases per group, n=28-31 cells/group) and motor cortex (control, 1446909 AU; *C9orf72*, 1692501 AU, n=2 cases per group, n=29-30 cells per group; Student's t-test; *$p < 0.05$, ****$p \leq 0.0001$). The increase in EEA1 fluorescence intensity was larger in the frontal cortex compared to the motor

cortex. (**e**-**f**; **m**-**n**) Control and *C9orf72* ALS/FTD microglia stained for Iba-1, Lamp1 and DAPI in areas of the frontal and motor cortex of *C9orf72* ALS/FTD patients. Scale bar, 5µm. (**g**,**o**) Extended view image of *C9orf72* ALS/FTD microglia show Lamp1 accumulations inside microglia in both frontal and motor cortex. Scale bar, 5µm. (**h**, **p**) A significant increase in Lamp1 mean intensity was also observed in microglia of the frontal cortex (mean fluorescence intensity in control, 1829123 AU; *C9orf72*, 4344005 AU; n=2 cases per group, n=31-32 cells per group) and motor cortex (control, 2894860 AU; *C9orf72,* 4559764 AU; n=2 cases per group, n=31-32 cells per group; Student's t-test; ****$p \leq 0.0001$). Data is presented as the Mean ± SEM.

Additional Files

Additional File 1: Figure S1. Expression of microglia specific genes and protein markers in control and *C9orf72* ALS/FTD iPSC-derived microglia**.** (**a**) Percentage of mature healthy control (n=3-5 lines) and *C9orf72* ALS/FTD (n=3-6 lines) iPSC-MG positive for P2ry12, Cx3cr1, TREM2 and TMEM119 protein markers. (**b**) Dot plots showing the level of expression as Log2 (counts +1) of microglia specific genes *spI1* (encodes for myeloid transcription factor PU.1), *p2ry12*, *cx3cr1*, *TREM2* and *TMEM119* in healthy control and *C9orf72* ALS/FTD (Control, n=4 lines, 1-2 differentiations per line; *C9orf72*, n=7 lines, 1-2 differentiations per line).

Additional File 2: Figure S2. Differentially expressed transcripts in *C9orf72* ALS/FTD versus control iPSC MG and postmortem tissues. (**a**) Top differentially expressed transcripts in iPSC MG full transcriptome (unadjusted p value <0.005; $\log_2$ fold change (FC) ± 1). (**b**) Top microglia-enriched dysregulated transcripts in the frontal and motor cortex of *C9orf72* ALS/FTD patient

tissue from bulk RNA sequencing. (**c**) Volcano plot of differentially expressed microglia-enriched genes (total of 881 from (52)) in *C9orf72* ALS/FTD occipital cortex (control, n=4 lines; *C9orf72*, n=5 lines) (unadjusted p value <0.005; $\log_2$ fold change (FC) ± 1). (**d**) Dysregulated transcripts in the occipital cortex of *C9orf72* ALS/FTD patient tissue from bulk RNA sequencing. All human brain RNA sequencing data was taken from Target ALS/NYGC.

Additional File 3: Figure S3. Differentially expressed genes from the complete transcriptome of *C9orf72* ALS/FTD patient tissue versus healthy control. (**a**-**b**) Dysregulated genes in the frontal and motor cortex of *C9orf72* ALS/FTD patient tissue from bulk RNA sequencing. RNA sequencing data taken from Target ALS/NYGC.

Additional File 4: Figure S4. *C9orf72* ALS/FTD iPSC-MG do not present TDP-43 pathology or mislocalization of ADAR2 to the cytoplasm**.** (**a**) Western Blot stripped and re-probe for tubulin. Tubulin was used the internal protein control to normalized human C9orf72 protein expression. (**b**) TDP-43 nuclear staining in control and *C9orf72* ALS/FTD iPSC-MG (control and *C9orf72*, n=2 lines per group, n = 60-84 iPSC-MG cells per line). IPSC-MG cell surface is outlined. Scale bar 15*μ*m. (**c**) Quantification of TDP-43 nucleocytoplasmic ratio. No evidence of cytoplasmic accumulations in *C9orf72* ALS/FTD iPSC-MG monocultures (control and *C9orf72* n=2 lines, n=60-84 cells per line; p= 0.7, Student's t-test). (**d**) Control and *C9orf72* ALS/FTD iPSC-MG immunostained for anti-ADAR2. IPSC-MG cell surface (white) and nuclear surface (blue) is outlined. Scale bar 10*μ*m. (**e**) Quantification of ADAR2 nucleocytoplasmic ratio. No evidence of

nuclear ADAR2 mislocalization to the cytoplasm was observed in *C9orf72* ALS/FTD iPSC-MG monocultures (control and *C9orf72* n=2 lines, n=100-115 cells per line; p=0.07, Student's t-test).

Additional File 5: Figure S5. Human brain synaptoneurosomes contain PSD95 and Synaptophysin 38 proteins from pre- and post- synaptic compartments. (**a**) Western blot analysis for total homogenate (TH) and synaptoneurosome preparations (SN). Four different SN preparations (TH1-TH4 and SN1-SN4) from four different control brains frozen samples. Preparations 1, 3 and 4 had successful enrichment of post-synaptic density 95 (PSD95 – 95kDa) and synaptophysin (Synaptophysin 38kDa) compared to total homogenate. In addition, low levels of nuclear marker histone 3 were observed in the SN preparations 1, 3, 4. SN1 (white arrow; TH1 and SN1) was the preparation used for the present study. (**b**) PSD95, synaptophysin 38 and Histone 3 quantification for TH and SN preparations 1, 3 and 4. A significant decrease in Histone 3 levels is observed in all SN preparations, p-value =0.02, Student's t-test.

Additional File 6: Figure S6. Time lapse imaging of *C9orf72* ALS/FTD iPSC-MG engulfing and degrading human synaptoneurosomes pHrodo (hSN-rodo). Selected representative images of *C9orf72* ALS/FTD iPSC-MG during time lapse live cell imaging of hSN-rodo engulfment. IPSC-MGs were labeled with the live nuclear marker Hoechst (blue) to identify individual cells followed by treatment with hSN-rodo (red). Fluorescent live cell imaging with differential interference contrast microscopy was performed over a 6 h time frame with images taken every 10 min. Here, we present selected images during the T0-T2h time point where more than 60% of iPSC-MGs engulf synapses. HSN-rodo are engulfed rapidly (white arrows highlight several phagocytic

iPSC-MGs) and an increase in hSN-rodo intensity is observed in individual cells indicating the uptake of hSN-rodo into acidic intracellular compartments.

Additional File 7: Table S1-S6

Table S1. Demographics for *C9orf72* ALS/FTD patient and control iPSCs

Table S2. Presence of *C9orf72* HRE in iPSC and iPSC-MG cells

Table S3. List of iPSC lines used for specific experiments

Table S4. Postmortem tissue sample IDs used for bulk RNA-seq analysis from Target ALS collection

Table S5. *C9orf72* ALS/FTD patient demographics for tissues used for immunostaining staining from Target ALS collection

Table S6. List of antibodies used to stain iPSC-MG cells

Additional File 8: Movie S1. Time lapse live imaging of *C9orf72* ALS/FTD iPSC-MG engulfing and degrading human synaptoneurosomes pHrodo (hSN-rodo)

Here, we present selected time lapse live cell imaging of *C9orf72* ALS/FTD iPSC-MG engulfing hSN-rodo. Fluorescent live cell imaging with differential interference contrast microscopy was performed over a 6 h time frame with images taken every 10 min. IPSC-MGs were identified using nuclear marker Hoechst (blue) followed by treatment with hSN-rodo (red). The increase in hSN-rodo intensity is observed in individual cells indicative of the uptake of hSN-rodo into acidic intracellular compartments for degradation.

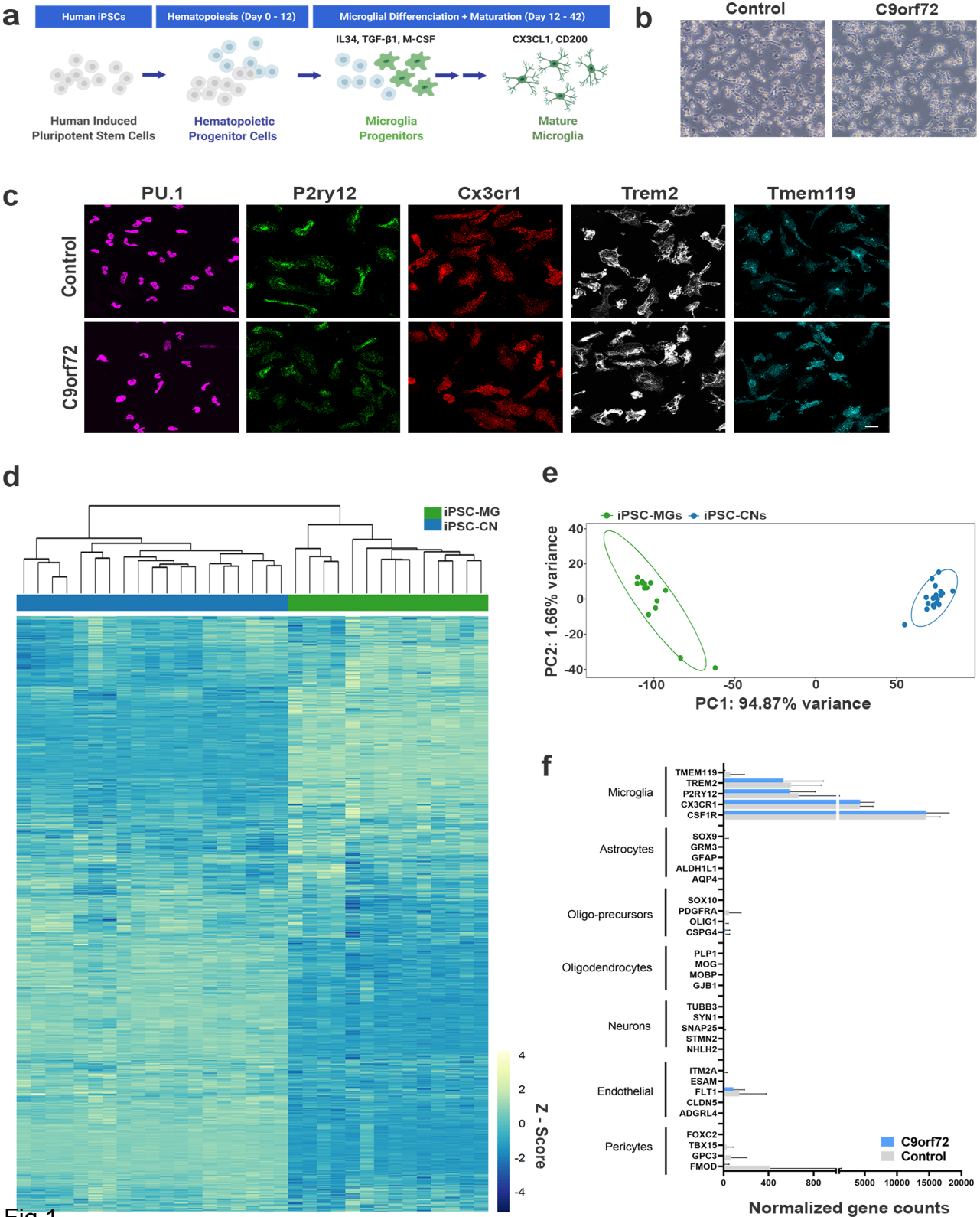
a
Human iPSCs
Hematopoiesis (Day 0 - 12)
Microglial Differenciation + Maturation (Day 12 - 42)
IL34, TGF-β1, M-CSF
CX3CL1, CD200
Human Induced Pluripotent Stem Cells
Hematopoietic Progenitor Cells
Microglia Progenitors
Mature Microglia
b
Control
C9orf72
c
PU.1
P2ry12
Cx3cr1
Trem2
Tmem119
Control
C9orf72
d
iPSC-MG
iPSC-CN
Z - Score
4
2
0
-2
-4
e
iPSC-MGs
iPSC-CNs
PC2: 1.66% variance
PC1: 94.87% variance
40
20
0
-20
-40
-100
-50
0
50
f
Microglia
TMEM119
TREM2
P2RY12
CX3CR1
CSF1R
Astrocytes
SOX9
GRM3
GFAP
ALDH1L1
AQP4
Oligo-precursors
SOX10
PDGFRA
OLIG1
CSPG4
Oligodendrocytes
PLP1
MOG
MOBP
GJB1
Neurons
TUBB3
SYN1
SNAP25
STMN2
NHLH2
Endothelial
ITM2A
ESAM
FLT1
CLDN5
ADGRL4
Pericytes
FOXC2
TBX15
GPC3
FMOD
C9orf72
Control
0
400
800
5000
10000
15000
20000
Normalized gene counts

Fig 1

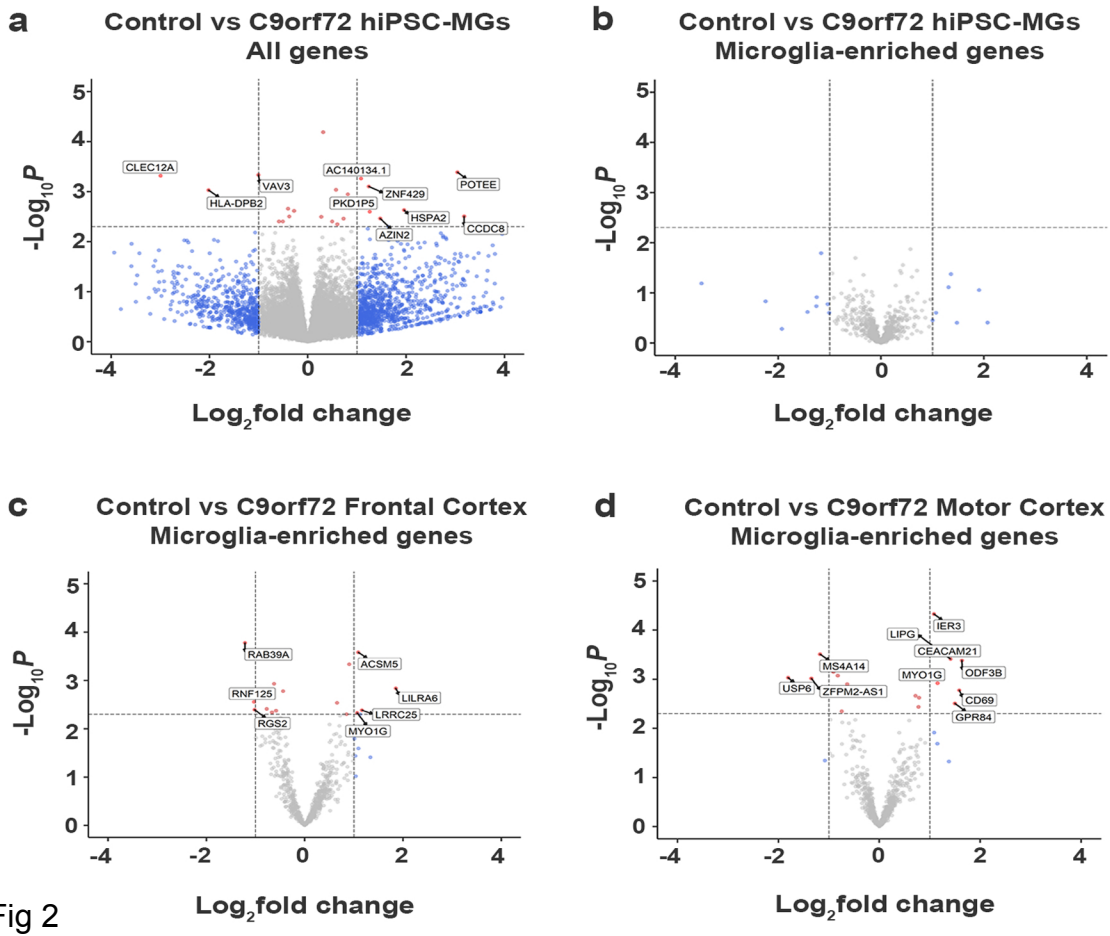
a
Control vs C9orf72 hiPSC-MGs
All genes
CLEC12A
VAV3
HLA-DPB2
AC140134.1
ZNF429
PKD1P5
HSPA2
AZIN2
POTEE
CCDC8
-Log10P
Log2fold change
b
Control vs C9orf72 hiPSC-MGs
Microglia-enriched genes
-Log10P
Log2fold change
c
Control vs C9orf72 Frontal Cortex
Microglia-enriched genes
RAB39A
RNF125
RGS2
ACSM5
LILRA6
LRRC25
MYO1G
-Log10P
Log2fold change
d
Control vs C9orf72 Motor Cortex
Microglia-enriched genes
IER3
LIPG
CEACAM21
MS4A14
MYO1G
ODF3B
USP6
ZFPM2-AS1
CD69
GPR84
-Log10P
Log2fold change

Fig 2

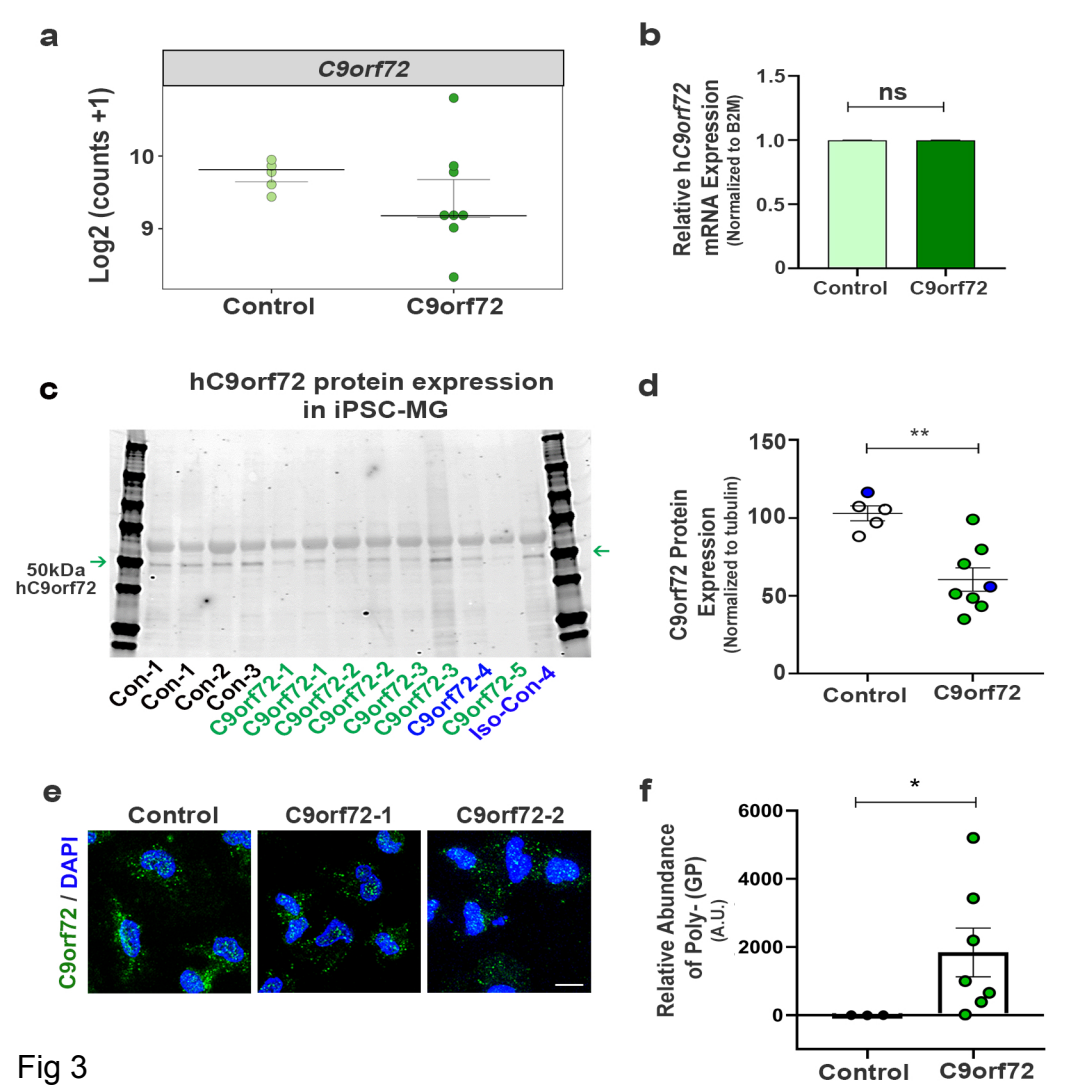
a
C9orf72
Log2 (counts +1)
10
9
Control
C9orf72
b
Relative hC9orf72 mRNA Expression
(Normalized to B2M)
1.5
1.0
0.5
0
ns
Control
C9orf72
c
hC9orf72 protein expression in iPSC-MG
50kDa hC9orf72
Con-1
Con-1
Con-2
Con-3
C9orf72-1
C9orf72-1
C9orf72-2
C9orf72-2
C9orf72-3
C9orf72-3
C9orf72-4
C9orf72-5
Iso-Con-4
d
C9orf72 Protein Expression
(Normalized to tubulin)
150
100
50
0
**
Control
C9orf72
e
Control
C9orf72-1
C9orf72-2
C9orf72 / DAPI
f
Relative Abundance of Poly- (GP)
(A.U.)
6000
4000
2000
0
*
Control
C9orf72

Fig 3

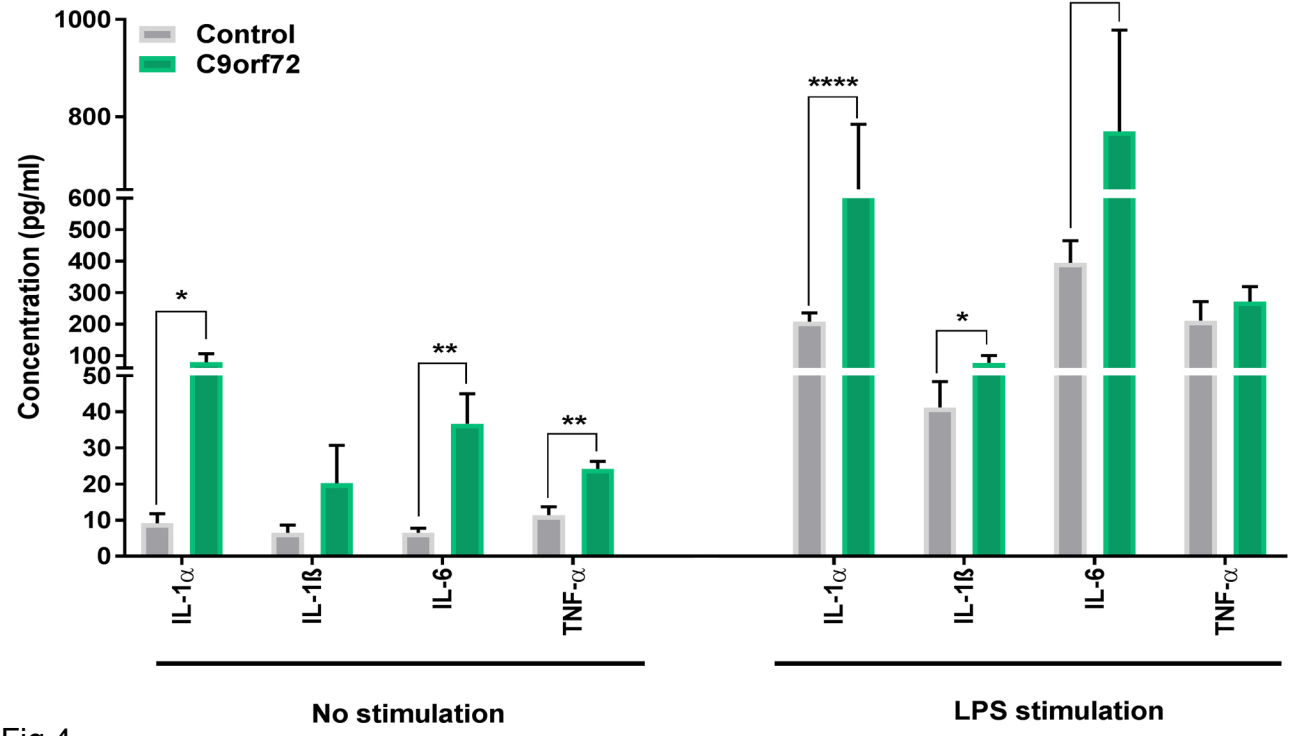
Control
C9orf72
Concentration (pg/ml)
1000
800
600
500
400
300
200
100
50
40
30
20
10
0
*
**
**
****
*
**
IL-1α
IL-1ß
IL-6
TNF-α
IL-1α
IL-1ß
IL-6
TNF-α
No stimulation
LPS stimulation

Fig 4

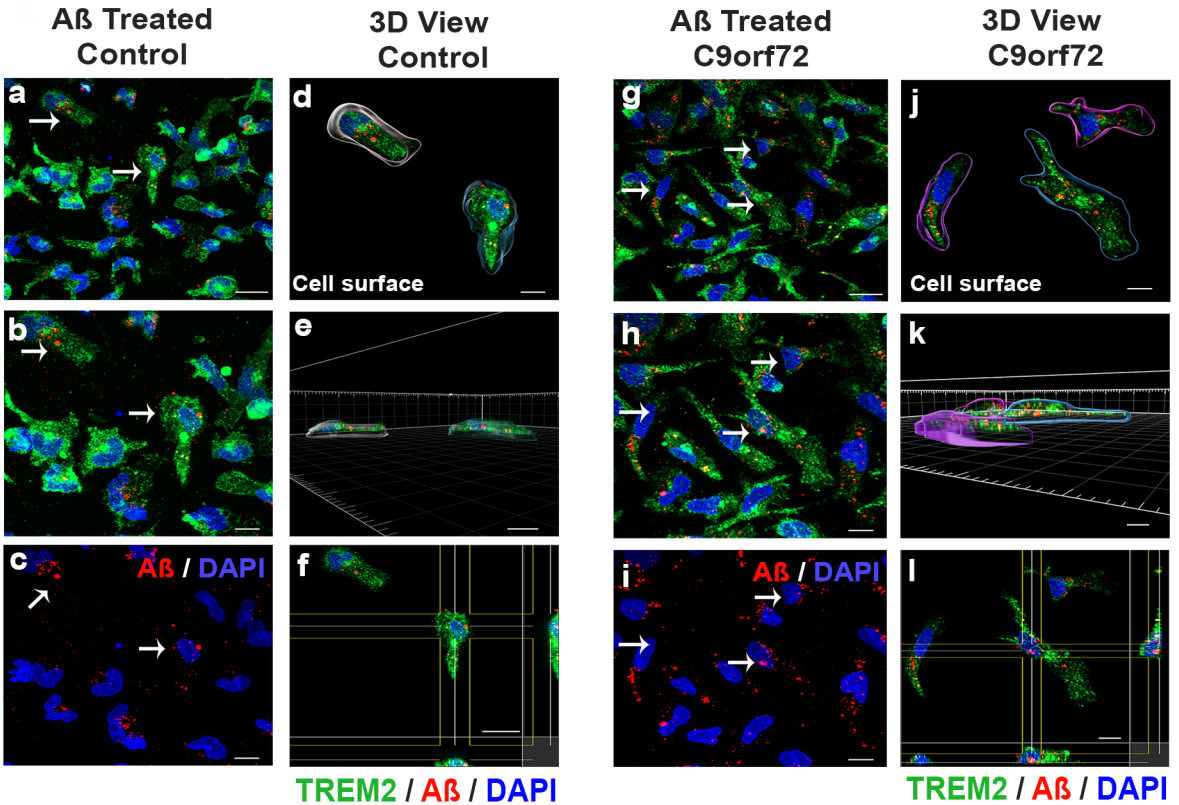
Aß Treated Control
3D View Control
Aß Treated C9orf72
3D View C9orf72
a
b
c
d
e
f
g
h
i
j
k
l
Cell surface
Cell surface
Aß / DAPI
Aß / DAPI
TREM2 / Aß / DAPI
TREM2 / Aß / DAPI

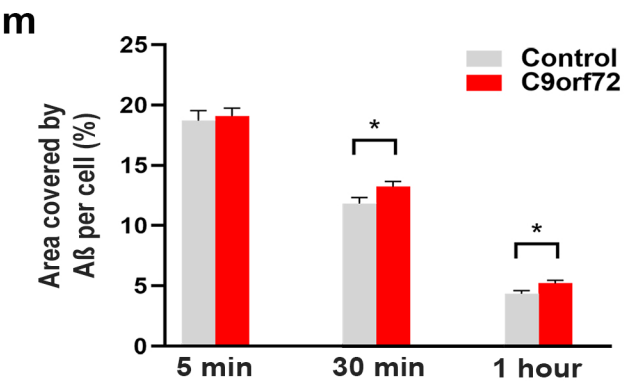
m
Area covered by Aß per cell (%)
25
20
15
10
5
0
Control
C9orf72
*
*
5 min
30 min
1 hour

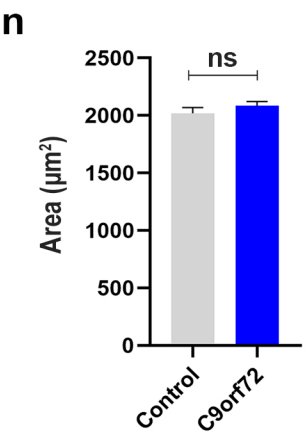
n
Area (µm²)
2500
2000
1500
1000
500
0
ns
Control
C9orf72

Fig 5

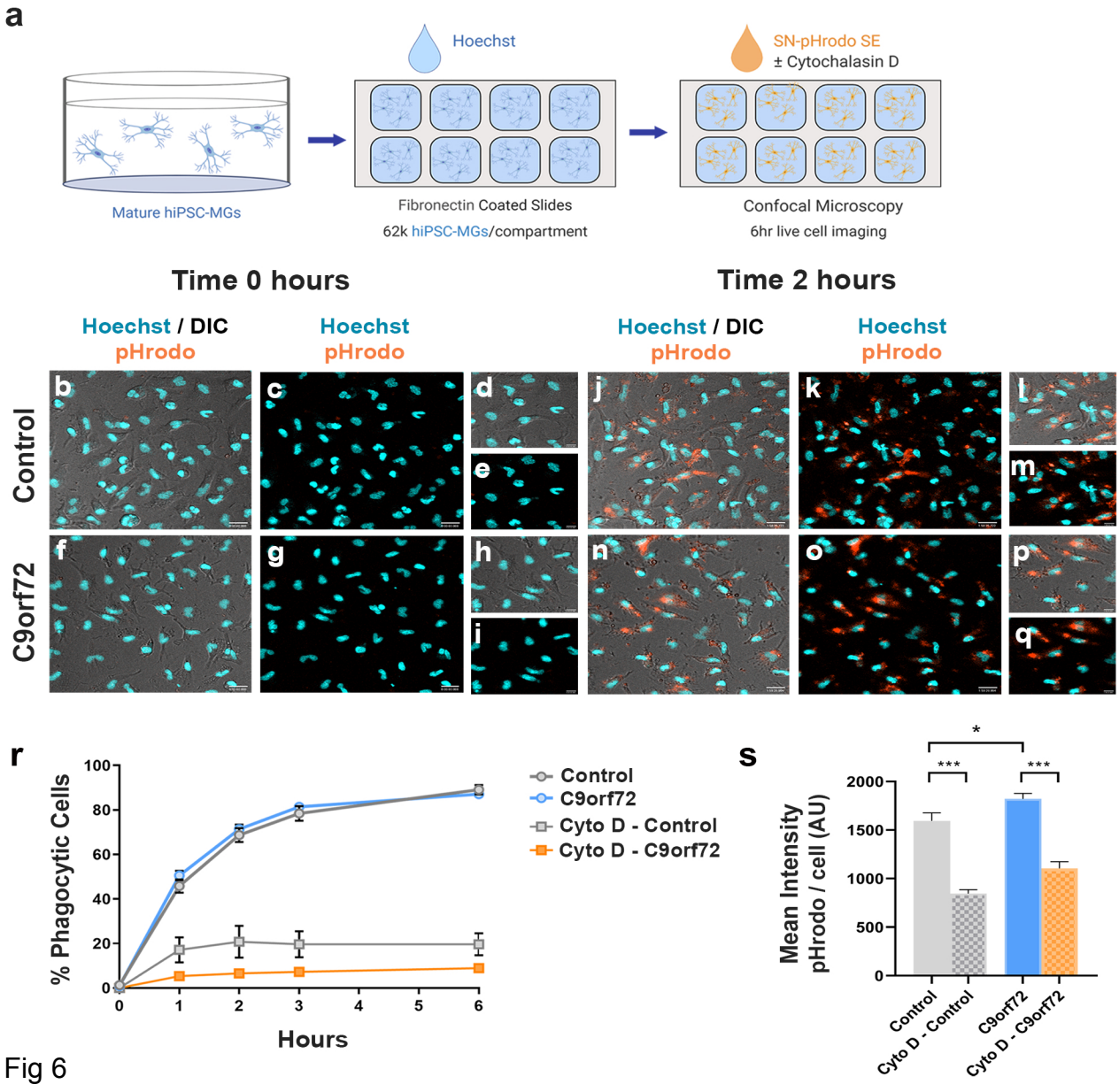
a
Hoechst
SN-pHrodo SE
± Cytochalasin D
Mature hiPSC-MGs
Fibronectin Coated Slides
62k hiPSC-MGs/compartment
Confocal Microscopy
6hr live cell imaging
Time 0 hours
Time 2 hours
Hoechst / DIC
pHrodo
Hoechst
pHrodo
Control
C9orf72
b
c
d
e
f
g
h
i
j
k
l
m
n
o
p
q
r
% Phagocytic Cells
Hours
Control
C9orf72
Cyto D - Control
Cyto D - C9orf72
s
Mean Intensity
pHrodo / cell (AU)
*
***
***
Control
Cyto D - Control
C9orf72
Cyto D - C9orf72

Fig 6

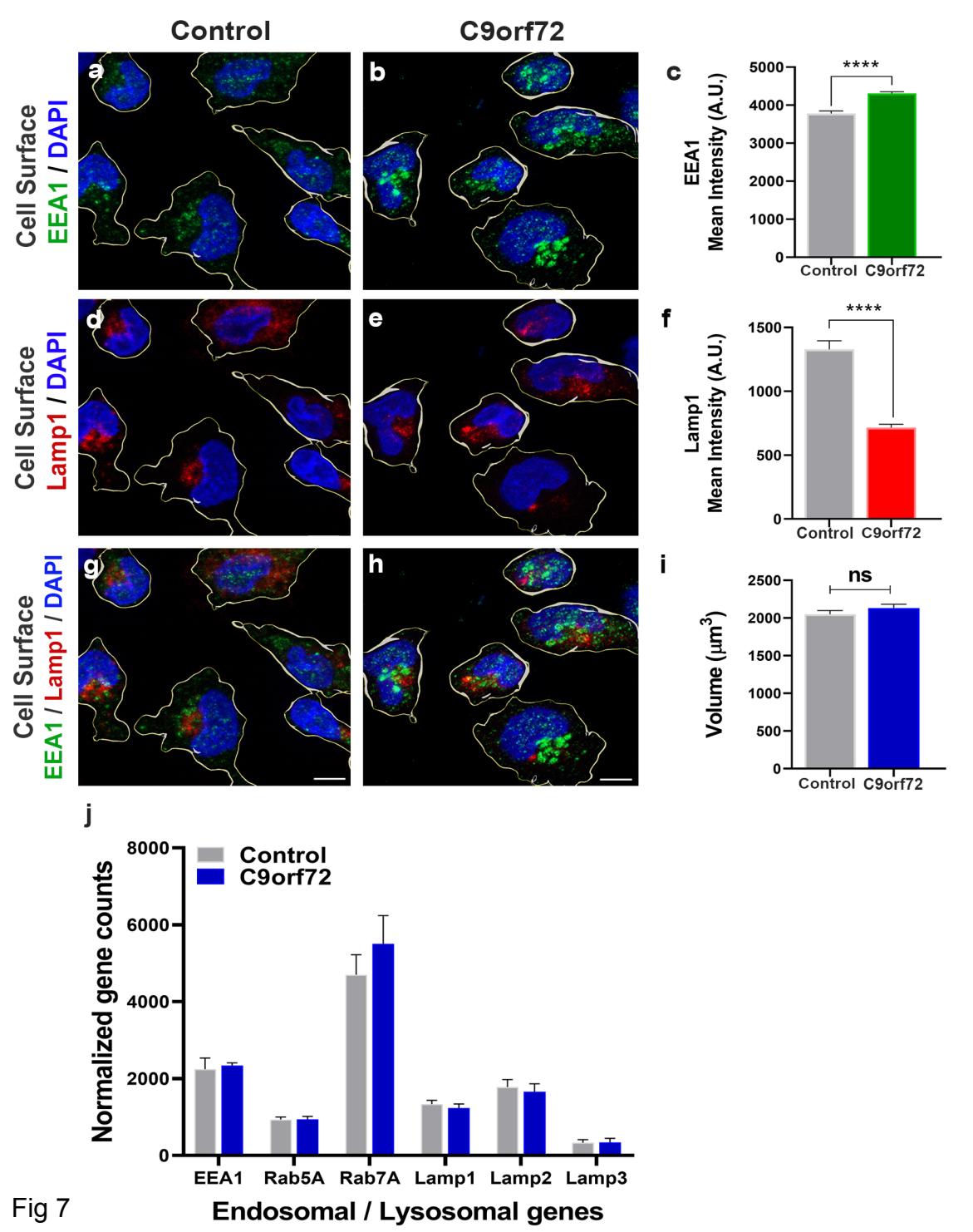
Control
C9orf72
a
b
c
d
e
f
g
h
i
j
Cell Surface
EEA1 / DAPI
Lamp1 / DAPI
EEA1 / Lamp1 / DAPI
EEA1 Mean Intensity (A.U.)
Lamp1 Mean Intensity (A.U.)
Volume (μm3)
****
ns
Control
C9orf72
Normalized gene counts
EEA1
Rab5A
Rab7A
Lamp1
Lamp2
Lamp3
Endosomal / Lysosomal genes

Fig 7

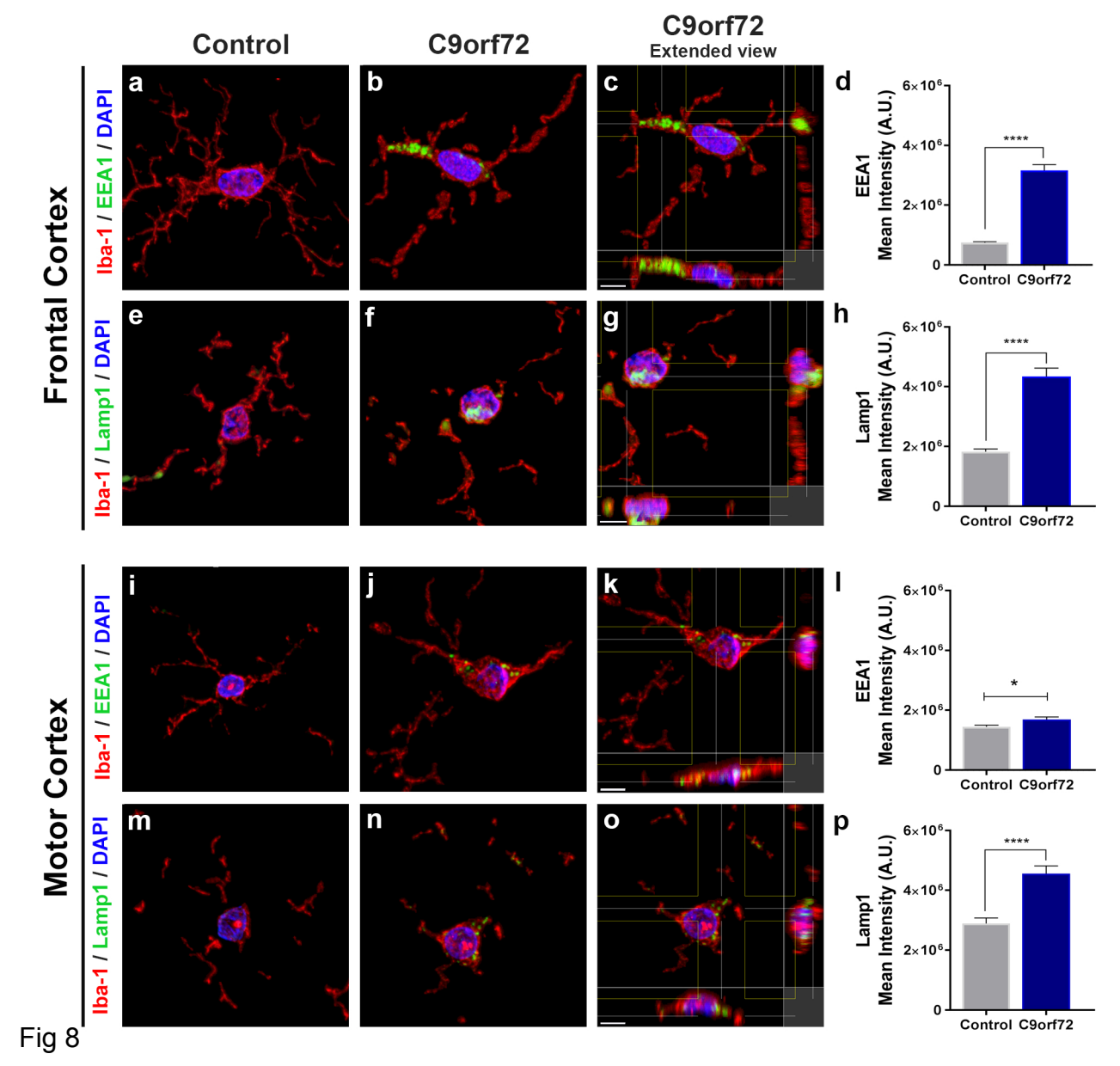
Control
C9orf72
C9orf72
Extended view
Frontal Cortex
Motor Cortex
Iba-1 / EEA1 / DAPI
Iba-1 / Lamp1 / DAPI
a
b
c
d
e
f
g
h
i
j
k
l
m
n
o
p
EEA1
Mean Intensity (A.U.)
Lamp1
Mean Intensity (A.U.)
6×10^6
4×10^6
2×10^6
0
****
*
Control
C9orf72

Fig 8

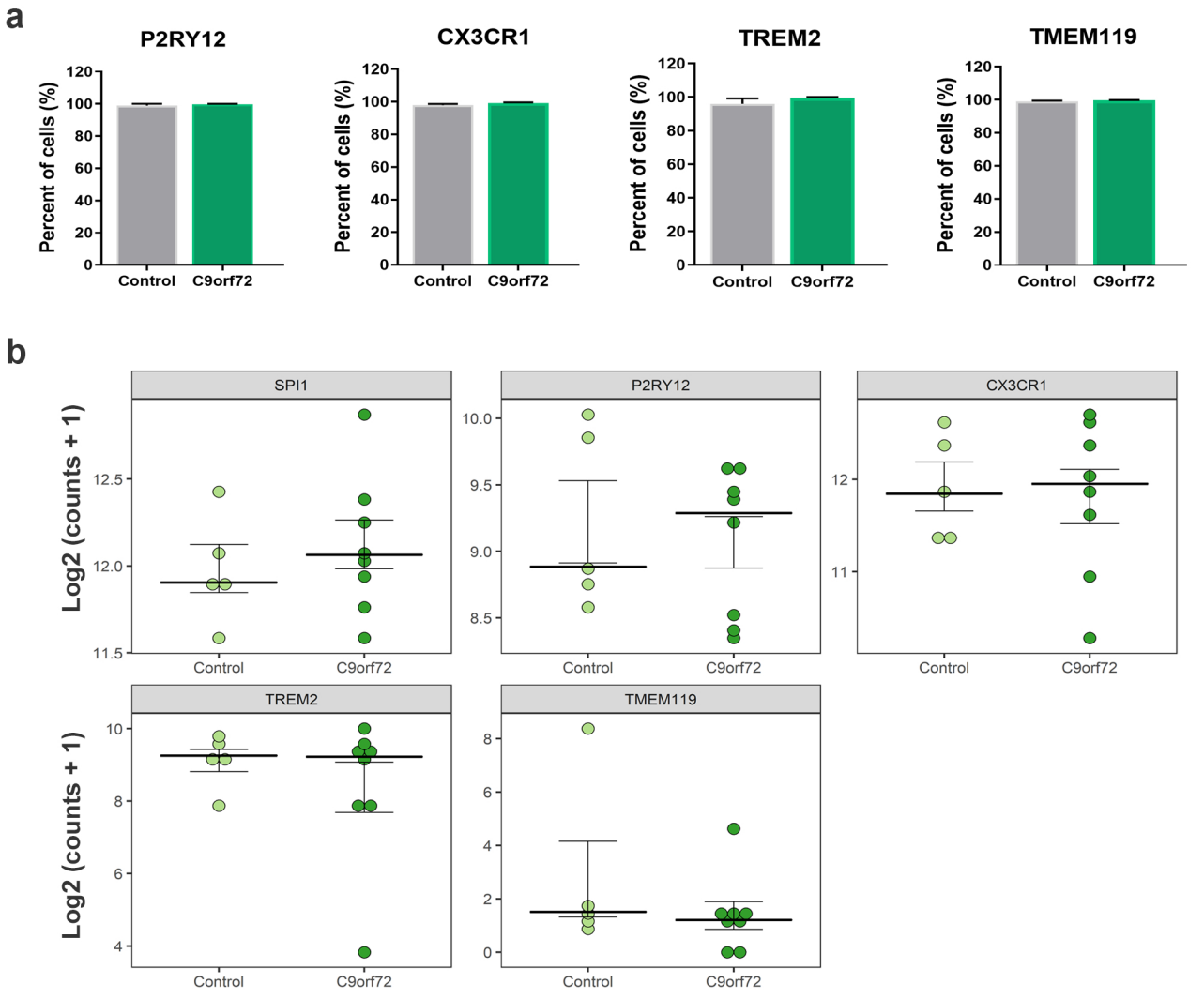
a
P2RY12
CX3CR1
TREM2
TMEM119
Percent of cells (%)
Control
C9orf72
b
SPI1
P2RY12
CX3CR1
TREM2
TMEM119
Log2 (counts + 1)
Control
C9orf72

Fig S1

a **Top differentially expressed genes in *C9orf72* ALS/FTD versus healthy control iPSC-MGs full transcriptome**

GeneID	Mean Expression	log2FoldChange	pvalue	Function
HOGA1	35.99377933	10.02954833	1.02E-03	4-hydroxy-2-oxoglutarate aldolase 1
SEC14L5	8.302217625	5.668051584	3.83E-04	SEC14 like lipid binding 5
AL021068.2	14.37981233	5.25019299	4.75E-04	ATP synthase 6 (MTATP6) pseudogene
TSPAN18	11.22990104	5.232275633	9.32E-05	tetraspanin 18
FPR3	32.81832265	4.357748152	6.77E-05	formyl peptide receptor 3
HERC2P8	6.942132063	4.292452758	2.15E-04	hect domain and RLD 2 pseudogene 8
PRSS8	2.886136682	4.058494716	1.16E-03	serine protease 8
CCDC8	52.12108214	3.181835055	3.12E-03	coiled-coil domain containing 8
POTEE	110.9768091	3.044353039	4.12E-04	POTE ankyrin domain family member E
HSPA2	12.72024179	1.958992029	2.35E-03	heat shock protein family A (Hsp70) member 2
AZIN2	16.20028104	1.472620525	3.45E-03	antizyme inhibitor 2
PKD1P5	39.83807692	1.259692119	2.52E-03	polycystin 1, transient receptor potential channel interacting pseudogene 5
ZNF429	43.95718957	1.242258356	7.92E-04	zinc finger protein 429
AC140134.1	60.66923167	1.084736579	5.49E-04	novel transcript, antisense to SMN2
VAV3	333.8017886	-1.004756607	4.64E-04	vav guanine nucleotide exchange factor 3
HLA-DPB2	16.03373275	-2.017725772	9.35E-04	major histocompatibility complex, class II, DP beta 2 (pseudogene)
CLEC12A	39.05534222	-2.992801595	4.80E-04	C-type lectin domain family 12 member A
L1TD1	16.48750267	-4.129676241	1.21E-04	LINE1 type transposase domain containing 1
AL592183.1	22.54644994	-4.350844446	7.74E-05	paralogue to a muscular dystrophy gene (frg1)
KCNK17	81.78711188	-7.423858968	1.97E-04	potassium two pore domain channel subfamily K member 17

b **Top differentially expressed microglia-enriched genes in brain regions affected by *C9orf72* ALS/FTD**
Patient tissue RNAseq from Target ALS

Frontal Cortex

GeneID	Mean Expression	log2FoldChange	pvalue	Function
ACSM5	65.2520943	1.089706576	2.62E-04	acyl-CoA synthetase medium chain family member 5
LILRA6	8.242638904	1.855077798	1.46E-03	leukocyte immunoglobulin like receptor A6
LRRC25	14.1927915	1.166641731	4.13E-03	leucine rich repeat containing 25
MYO1G	41.87188372	1.070172293	4.72E-03	myosin IG
RAB39A	81.5794358	-1.213506643	1.67E-04	RAB39A, member RAS oncogene family
RGS2	264.235745	-1.017507335	4.04E-03	regulator of G protein signaling 2
RNF125	76.50144549	-1.031177183	2.78E-03	ring finger protein 125

Motor Cortex

GeneID	Mean Expression	log2FoldChange	pvalue	Function
CD69	14.39047314	1.585646223	1.68E-03	CD69 molecule
CEACAM21	12.52373946	1.241529322	2.83E-04	CEA cell adhesion molecule 21
GPR84	12.81951259	1.500018857	3.11E-03	G protein-coupled receptor 84
IER3	37.27390214	1.081831413	4.71E-05	immediate early response 3
LIPG	24.75216691	1.411126078	3.90E-04	lipase G, endothelial type
MS4A14	55.54576753	-1.175313395	3.11E-04	membrane spanning 4-domains A14
MYO1G	39.2124265	1.155664159	1.20E-03	myosin IG
ODF3B	17.17098378	1.637140954	4.17E-04	outer dense fiber of sperm tails 3B
USP6	15.80529876	-1.80830343	9.32E-04	ubiquitin specific peptidase 6
ZFPM2-AS1	17.0065677	-1.347531569	9.65E-04	ZFPM2 antisense RNA 1

c

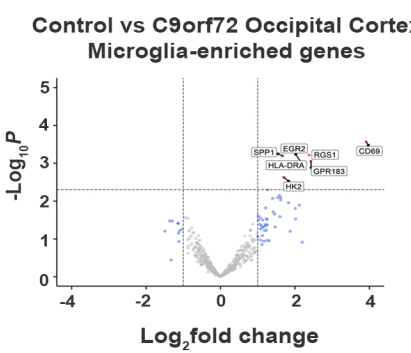

d **Occipital Cortex**

GeneID	Mean Expression	log2FoldChange	pvalue	Function
CD69	11.11028823	3.914411706	2.71E-04	CD69 molecule
EGR2	49.22298544	2.163956311	9.37E-04	early growth response 2
GPR183	18.4898987	2.429522603	8.83E-04	G protein-coupled receptor 183
HK2	258.2353303	1.702312412	2.36E-03	hexokinase 2
HLA-DRA	212.4528805	1.860607336	1.39E-03	major histocompatibility complex, class II, DR alpha
RGS1	146.5013827	2.383177621	6.07E-04	regulator of G protein signaling 1
SPP1	3323.737197	1.671517957	6.38E-04	secreted phosphoprotein 1

Fig S2

Top differentially expressed genes from complete transcriptome of *C9orf72* ALS/FTD patient tissue versus healthy control

a

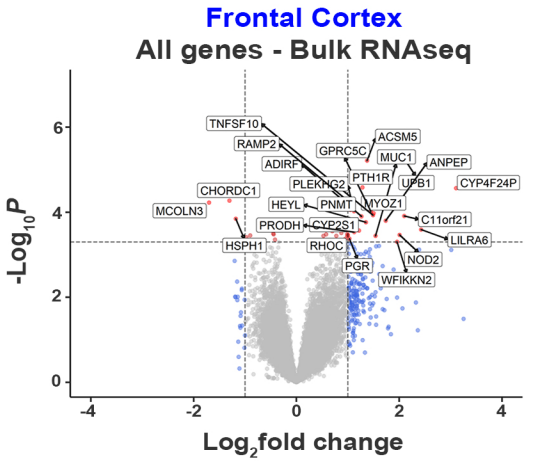

GeneID	Mean Expression	log2FoldChange	pvalue	Function
ACSM5	68.12888197	1.373696141	6.11E-06	acyl-CoA synthetase medium chain family member 5
UPB1	14.47883617	2.140602571	6.57E-06	beta-ureidopropionase 1
PTH1R	143.2963167	1.285612142	2.62E-05	parathyroid hormone 1 receptor
CYP4F24P	18.92983176	3.107071242	2.71E-05	cytochrome P450 family 4 subfamily F member 24, pseudogene
CHORDC1	1690.20189	-1.30139591	5.33E-05	cysteine and histidine rich domain containing 1
MCOLN3	12.78944298	-1.699498265	5.94E-05	mucolipin 3
RAMP2	32.25448123	1.09412786	6.76E-05	receptor activity modifying protein 2
PNMT	43.82179614	1.049248911	8.83E-05	phenylethanolamine N-methyltransferase
PLEKHG2	88.19394237	1.118928092	9.54E-05	pleckstrin homology and RhoGEF domain containing G2
GPRC5C	121.5717407	1.448077342	9.72E-05	G protein-coupled receptor class C group 5 member C
MYOZ1	11.26405499	1.500475718	1.06E-04	myozenin 1
TNFSF10	47.69956595	1.490896485	1.18E-04	TNF superfamily member 10
C11orf21	16.84168556	2.095358277	1.23E-04	chromosome 11 open reading frame 21
ADIRF	197.0590585	1.267162951	1.26E-04	adipogenesis regulatory factor
HSPH1	5083.178638	-1.18017007	1.42E-04	heat shock protein family H (Hsp110) member 1
ANPEP	23.01343049	1.737089039	1.58E-04	alanyl aminopeptidase, membrane
HEYL	85.64350354	1.354272338	1.72E-04	hes related family bHLH transcription factor with YRPW motif like
LILRA6	10.24372236	2.424695542	2.56E-04	leukocyte immunoglobulin like receptor A6
CYP2S1	14.890158	1.216256243	2.71E-04	cytochrome P450 family 2 subfamily S member 1
PRODH	1383.260451	1.124011128	2.93E-04	proline dehydrogenase 1

b

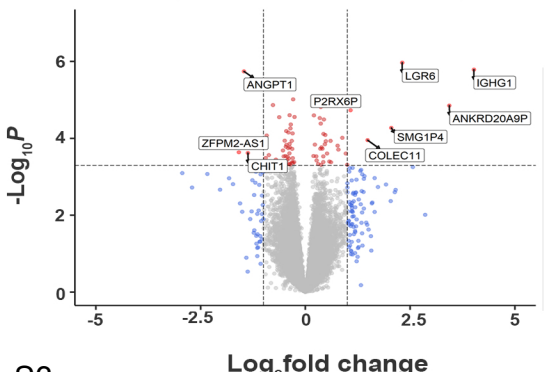

GeneID	Mean Expression	log2FoldChange	lfcSE	pvalue	Function
LGR6	32.9179496	2.314623327	0.474599	1.08E-06	leucine rich repeat containing G protein-coupled receptor 6
IGHG1	13.15030401	4.023116643	0.839139	1.63E-06	immunoglobulin heavy constant gamma 1 (G1m marker)
ANGPT1	135.674109	-1.462922571	0.30652	1.82E-06	angiopoietin 1
ANKRD20A9P	15.8352823	3.43383058	0.790833	1.41E-05	ankyrin repeat domain 20 family member A9, pseudogene
P2RX6P	33.22564559	1.080468933	0.252412	1.86E-05	purinergic receptor P2X 6 pseudogene
SMG1P4	31.88047041	2.049123316	0.507014	5.31E-05	SMG1 pseudogene 4
COLEC11	25.33189606	1.484945093	0.384307	1.12E-04	collectin subfamily member 11
ZFPM2-AS1	18.29770547	-1.587667615	0.431019	2.30E-04	ZFPM2 antisense RNA 1
CHIT1	20.60728413	-1.369519087	0.3729	2.40E-04	chitinase 1
CXCL11	9.4661815	2.563451188	0.743041	5.61E-04	C-X-C motif chemokine ligand 11
FAAHP1	22.50310124	1.124049813	0.327082	5.89E-04	fatty acid amide hydrolase pseudogene 1
IER3	39.26479111	1.061020716	0.309023	5.96E-04	immediate early response 3

Fig S3

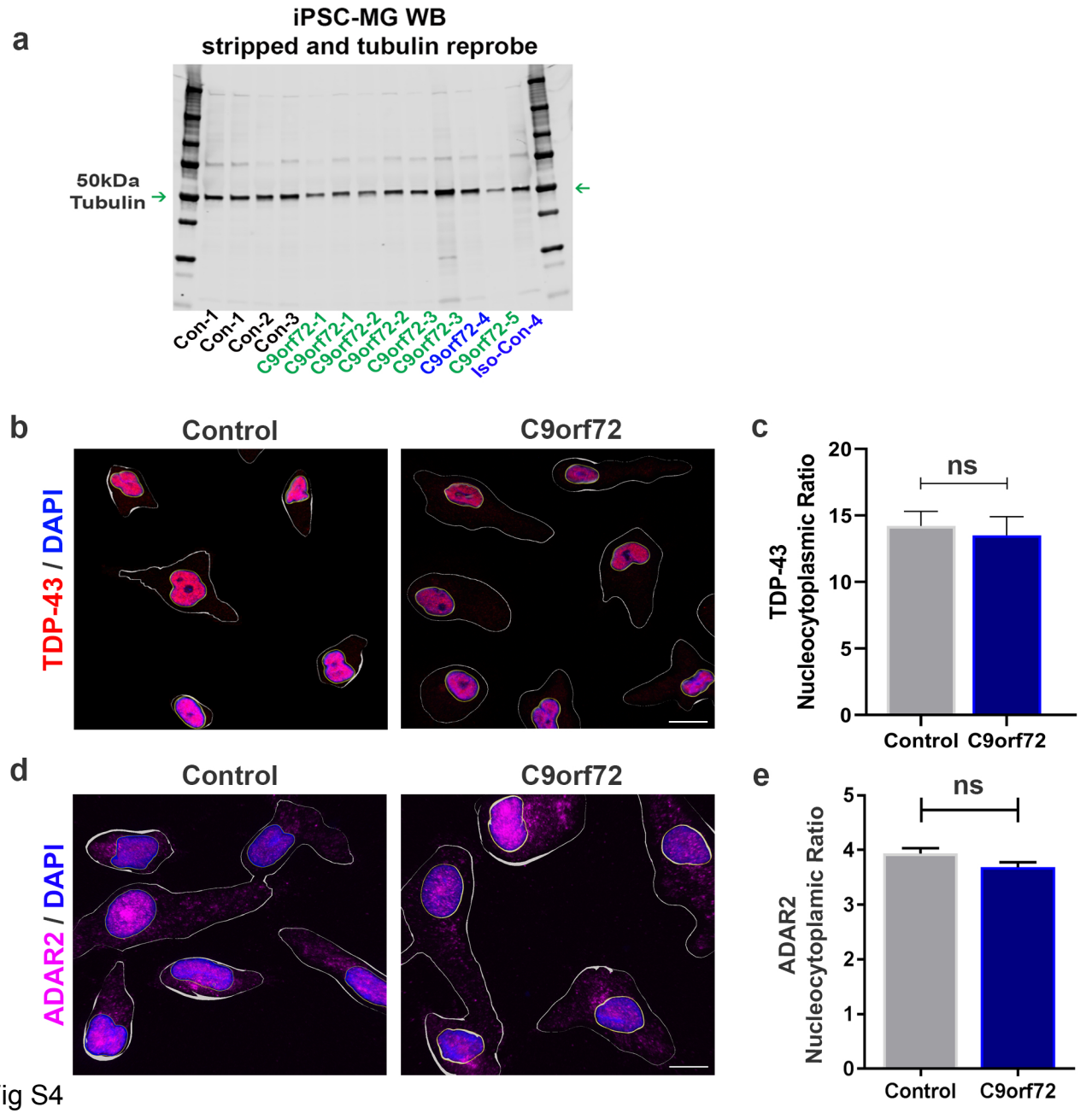
a
iPSC-MG WB
stripped and tubulin reprobe
50kDa
Tubulin
Con-1
Con-1
Con-2
Con-3
C9orf72-1
C9orf72-1
C9orf72-2
C9orf72-2
C9orf72-3
C9orf72-3
C9orf72-4
C9orf72-5
Iso-Con-4
b
Control
C9orf72
TDP-43 / DAPI
c
TDP-43
Nucleocytoplasmic Ratio
ns
20
15
10
5
0
Control
C9orf72
d
Control
C9orf72
ADAR2 / DAPI
e
ADAR2
Nucleocytoplamic Ratio
ns
5
4
3
2
1
0
Control
C9orf72

Fig S4

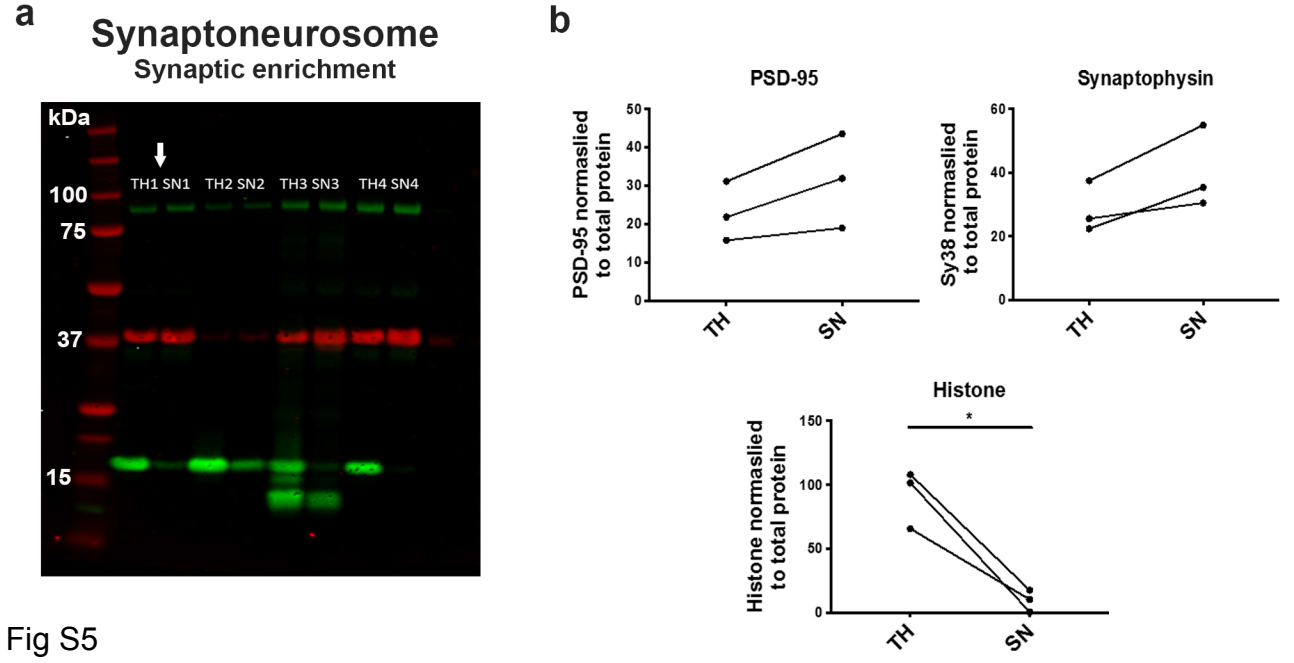
a
Synaptoneurosome
Synaptic enrichment
kDa
100
75
37
15
TH1 SN1
TH2 SN2
TH3 SN3
TH4 SN4
b
PSD-95
PSD-95 normaslied to total protein
50
40
30
20
10
0
TH
SN
Synaptophysin
Sy38 normaslied to total protein
60
40
20
0
TH
SN
Histone
Histone normaslied to total protein
*
150
100
50
0
TH
SN

Fig S5

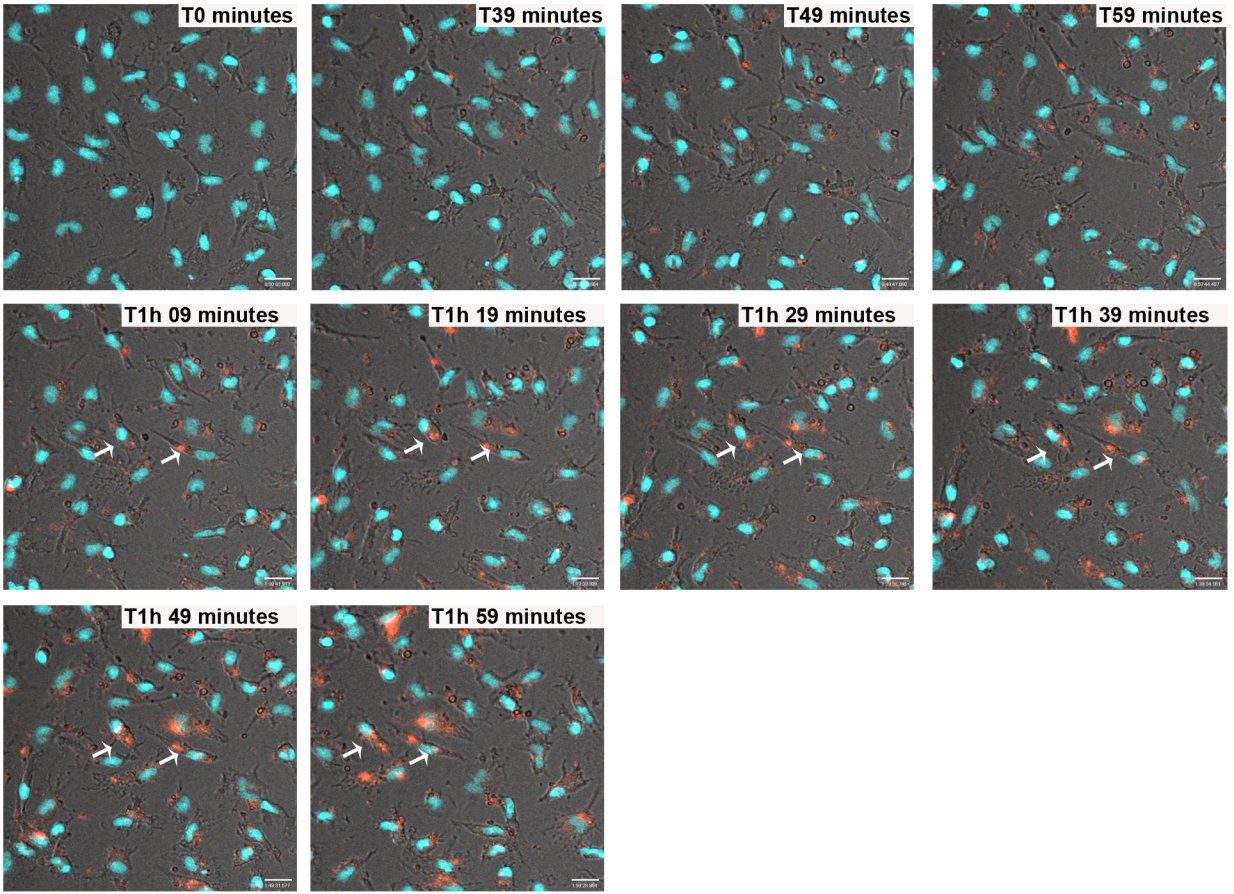
T0 minutes
T39 minutes
T49 minutes
T59 minutes
T1h 09 minutes
T1h 19 minutes
T1h 29 minutes
T1h 39 minutes
T1h 49 minutes
T1h 59 minutes

Fig S6

Additional File 7: Tables S1-S6

Table S1. Demographics for *C9orf72* ALS/FTD patient and healthy control iPSCs

iPSC line	Gene Mutation	C9 Expansion Size	Gender	Age at disease onset (yrs)	Age at biopsy/blood draw (yrs)	Age at death (yrs)	Disease duration (yrs)	Comments
C9orf72 -1	*C9orf72*	>30 repeats	Female	60	63	N/A	N/A	
C9orf72 -2	*C9orf72*	>30 repeats	Female	50	51	52	2	
C9orf72 -3	*C9orf72*	>30 repeats	*	*	*	N/A	N/A	Almeida et al, Acta Neuropathol, 2013
C9orf72 -4	*C9orf72*	>30 repeats	*	*	*	N/A	N/A	Lopez-Gonzalez et al, Neuron, 2016
C9orf72 -5	*C9orf72*	>30 repeats	*	*	*	N/A	N/A	Almeida et al, Acta Neuropathol, 2013
C9orf72 -6	*C9orf72*	>30 repeats	Male	52	58	N/A	N/A	
C9orf72 -7	*C9orf72*	>30 repeats	Male	48	51	59	11	
C9orf72 -8	*C9orf72*	>30 repeats	Male	57	58	59	1.7	
Control 1	Control	N/A	Female	N/A	N/A	N/A	N/A	
Control 2	Control	N/A	Male	N/A	N/A	N/A	N/A	
Control 3	Control	N/A	Male	N/A	N/A	N/A	N/A	
● Control 4	Isogenic Control	N/A	*	*	*	N/A	N/A	
Control 5	Control	N/A	Female	N/A	N/A	N/A	N/A	
Control 6	Control	N/A	Male	N/A	N/A	N/A	N/A	

*** - this information is not provided to protect the ID of the donors**

● C9orf72-4 isogenic pair

Table S2. Presence of *C9orf72* HRE in iPSC and iPSC-MG cells

			Repeat primed PCR
Cell Line	**Gene mutation**	**Cell Type**	**C9 HRE (>30)**
C9orf72-1	*C9orf72*	iPSC	Yes
		iPSC-MG	Yes
C9orf72-2	*C9orf72*	iPSC	Yes
		iPSC-MG	Yes
C9orf72-3	*C9orf72*	iPSC	Yes
		iPSC-MG	Yes
C9orf72-4	*C9orf72*	iPSC	Yes
		iPSC-MG	Yes
C9orf72-5	*C9orf72*	iPSC	not determined
		iPSC-MG	not determined
C9orf72-6	*C9orf72*	iPSC	Yes
		iPSC-MG	Yes
C9orf72-7	*C9orf72*	iPSC	Yes
		iPSC-MG	not determined
C9orf72-8	*C9orf72*	iPSC	not determined
		iPSC-MG	not determined
Control 1	Control	iPSC	No
		iPSC-MG	No
Control 2	Control	iPSC	not determined
		iPSC-MG	not determined
Control 3	Control	iPSC	No
		iPSC-MG	No
Control 4	Isogenic Control	iPSC	No
		iPSC-MG	No
Control 5	Control	iPSC	not determined
		iPSC-MG	not determined
Control 6	Control	iPSC	No
		iPSC-MG	not determined

Table S3. List of iPSC lines used for specific experiments

Cell Line	Gene mutation	RNAseq	MG markers	C9 HRE (>30)	qPCR - hC9	C9 Protein	Poly (GP)	TDP-43 ADAR2	Cytokine Analysis	Phagocytic Activity Aβ 1-40 TAMRA	hSN Assay hSN-rodo	EAA1/Lamp1 Basal Conditions
C9orf72-1	*C9orf72*	√	√	√	√	√	√	√	√	√	√	√
C9orf72-2	*C9orf72*	√	√	√	√	√	√			√		
C9orf72-3	*C9orf72*	√	√	√	√	√	√	√	√	√		
C9orf72-4	*C9orf72*	√	√	√	√	√	√					
C9orf72-5	*C9orf72*	√	√		√	√	√			√	√	
C9orf72-6	*C9orf72*	√	√	√	√		√					√
C9orf72-7	*C9orf72*	√	√									
C9orf72-8	*C9orf72*						√					
Control 1	Control	√	√	No	√	√	√	√	√	√		√
Control 2	Control	√	√		√	√		√	√			
Control 3	Control		√	No	√	√	√			√	√	√
Control 4	IsogenicControl			No			√					
Control 5	Control	√	√									
Control 6	Control	√	√						√			

Table S4. Postmortem tissue sample IDs used for bulk RNAseq analysis from Target ALS collection

Motor Cortex

ID	Tissue of Origin	Classification
CGND-HRA-00251	Cortex_Motor	Control
CGND-HRA-00218	Cortex_Motor	Control
CGND-HRA-00590	Cortex_Motor	Control
CGND-HRA-00224	Cortex_Motor	Control
CGND-HRA-00654	Cortex_Motor	Control
CGND-HRA-00569	Cortex_Motor	Control
CGND-HRA-00595	Cortex_Motor	Control
CGND-HRA-00091	Cortex_Motor	Control
CGND-HRA-00568	Cortex_Motor	Control
CGND-HRA-00063	Cortex_Motor	Control
CGND-HRA-01186	Cortex_Motor	Control
CGND-HRA-00594	Cortex_Motor	Control
CGND-HRA-00655	Cortex_Motor	Control
CGND-HRA-00596	Cortex_Motor	Control
CGND-HRA-01187	Cortex_Motor	Control
		15

CGND-HRA-00134	Cortex_Motor	C9ALS
CGND-HRA-00631	Cortex_Motor	C9ALS
CGND-HRA-00358	Cortex_Motor	C9ALS
CGND-HRA-00321	Cortex_Motor	C9ALS
CGND-HRA-00287	Cortex_Motor	C9ALS
CGND-HRA-00286	Cortex_Motor	C9ALS
CGND-HRA-00359	Cortex_Motor	C9ALS
CGND-HRA-00254	Cortex_Motor	C9ALS
CGND-HRA-00320	Cortex_Motor	C9ALS
CGND-HRA-00288	Cortex_Motor	C9ALS
CGND-HRA-00088	Cortex_Motor	C9ALS
CGND-HRA-00060	Cortex_Motor	C9ALS
		12

Frontal Cortex

ID	Tissue of Origin	Classification
CGND-HRA-01179	Cortex_Frontal	Control
CGND-HRA-00212	Cortex_Frontal	Control
CGND-HRA-01379	Cortex_Frontal	Control
CGND-HRA-00751	Cortex_Frontal	Control
CGND-HRA-00021	Cortex_Frontal	Control
CGND-HRA-00476	Cortex_Frontal	Control
CGND-HRA-01236	Cortex_Frontal	Control
CGND-HRA-00242	Cortex_Frontal	Control
CGND-HRA-01225	Cortex_Frontal	Control
CGND-HRA-00529	Cortex_Frontal	Control
CGND-HRA-01234	Cortex_Frontal	Control
CGND-HRA-01228	Cortex_Frontal	Control
CGND-HRA-00466	Cortex_Frontal	Control
CGND-HRA-01185	Cortex_Frontal	Control
CGND-HRA-00788	Cortex_Frontal	Control
CGND-HRA-00871	Cortex_Frontal	Control
		16

CGND-HRA-00018	Cortex_Frontal	C9ALS
CGND-HRA-00245	Cortex_Frontal	C9ALS
CGND-HRA-00362	Cortex_Frontal	C9ALS
CGND-HRA-00550	Cortex_Frontal	C9ALS
CGND-HRA-00323	Cortex_Frontal	C9ALS
CGND-HRA-00244	Cortex_Frontal	C9ALS
CGND-HRA-00248	Cortex_Frontal	C9ALS
CGND-HRA-00460	Cortex_Frontal	C9ALS
		8

Occipital Cortex

ID	Tissue of Origin	Classification
CGND-HRA-01204	Cortex_Occipital	Control
CGND-HRA-01343	Cortex_Occipital	Control
CGND-HRA-01235	Cortex_Occipital	Control
CGND-HRA-00567	Cortex_Occipital	Control
		4

CGND-HRA-00551	Cortex_Occipital	C9ALS
CGND-HRA-01337	Cortex_Occipital	C9ALS
CGND-HRA-00363	Cortex_Occipital	C9ALS
CGND-HRA-00540	Cortex_Occipital	C9ALS
CGND-HRA-00324	Cortex_Occipital	C9ALS
		5

Table S5. *C9orf72* ALS/FTD patient demographics for tissues used for immunostaining from Target ALS collection

ID	Genotype	R/G	DOD	Age of onset	Site of onset	Diagnosis	Cause of death
86	C9orf72	WM	74	67	Cognitive	FTD + fALS	
88	C9orf72	WM	59	57	Bulbar	FTD + fALS	
100	Control	ASN/F	52	N/A	N/A	N/A	Cardiac arrest
110	Control	M	50	N/A	N/A	N/A	hypertensive vasculopathy, hypoxia/ischemia

*R/G – Race and gender; *DOD – Date of death

Table S6. List of antibodies used to stained iPSC-MG cells

Antibodies	Source	Catalog Number	Concentration
Anti- PU.1	Cell Signaling Technologies	2266S	1:500
Anti-P2ry12	Sigma	HPA014518	1:500
Anti-CX3CR1	Biorad/AbD Serotec	AHP1589	1:500
Anti-Trem2	Abcam	ab209814	1:500
Anti-Tmem119	Abcam	ab185333	1:100
Anti-C9orf72	Sigma	HPA023873	1:100
Anti-TDP-43	Cell Signaling Technologies	89789 -D9R3L	1:500
Anti- ADAR2	Sigma	HPA018277	1:500
Anti-EEA1	BD Biosciences	610457	1:700
Anti-Lamp1	Developmental Hybridoma Bank	H4A3-s	1:100